



UNIVERSITY OF LEEDS

This is a repository copy of *Dynamic redox conditions control late Ediacaran metazoan ecosystems in the Nama Group, Namibia*.

White Rose Research Online URL for this paper:
<http://eprints.whiterose.ac.uk/84669/>

Version: Accepted Version

Article:

Wood, RA, Poulton, SW, Prave, AR et al. (9 more authors) (2015) Dynamic redox conditions control late Ediacaran metazoan ecosystems in the Nama Group, Namibia. *Precambrian Research*, 261. 252 - 271. ISSN 0301-9268

<https://doi.org/10.1016/j.precamres.2015.02.004>

(c) 2015, Elsevier. Licensed under the Creative Commons Attribution-NonCommercial-NoDerivatives 4.0 International
<http://creativecommons.org/licenses/by-nc-nd/4.0>

Reuse

Unless indicated otherwise, fulltext items are protected by copyright with all rights reserved. The copyright exception in section 29 of the Copyright, Designs and Patents Act 1988 allows the making of a single copy solely for the purpose of non-commercial research or private study within the limits of fair dealing. The publisher or other rights-holder may allow further reproduction and re-use of this version - refer to the White Rose Research Online record for this item. Where records identify the publisher as the copyright holder, users can verify any specific terms of use on the publisher's website.

Takedown

If you consider content in White Rose Research Online to be in breach of UK law, please notify us by emailing eprints@whiterose.ac.uk including the URL of the record and the reason for the withdrawal request.

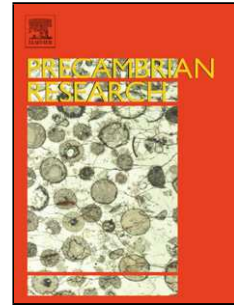


eprints@whiterose.ac.uk
<https://eprints.whiterose.ac.uk/>

Accepted Manuscript

Title: Dynamic redox conditions control late Ediacaran metazoan ecosystems in the Nama Group, Namibia

Author: R.A. Wood S.W. Poulton A.R. Prave K.-H. Hoffmann
M.O. Clarkson R. Guilbaud J.W. Lyne R. Tostevin F. Bowyer
A.M. Penny A. Curtis S.A. Kasemann



PII: S0301-9268(15)00045-5
DOI: <http://dx.doi.org/doi:10.1016/j.precamres.2015.02.004>
Reference: PRECAM 4193

To appear in: *Precambrian Research*

Received date: 21-7-2014
Revised date: 30-12-2014
Accepted date: 4-2-2015

Please cite this article as: Wood, R.A., Poulton, S.W., Prave, A.R., Hoffmann, K.-H., Clarkson, M.O., Guilbaud, R., Lyne, J.W., Tostevin, R., Bowyer, F., Penny, A.M., Curtis, A., Kasemann, S.A., Dynamic redox conditions control late Ediacaran metazoan ecosystems in the Nama Group, Namibia, *Precambrian Research* (2015), <http://dx.doi.org/10.1016/j.precamres.2015.02.004>

This is a PDF file of an unedited manuscript that has been accepted for publication. As a service to our customers we are providing this early version of the manuscript. The manuscript will undergo copyediting, typesetting, and review of the resulting proof before it is published in its final form. Please note that during the production process errors may be discovered which could affect the content, and all legal disclaimers that apply to the journal pertain.

Highlights

- New carbon isotope data capture the final stages of the Shuram/Wonoka excursion
- The transition to positive values postdates the appearance of calcified metazoans
- Anoxic ferruginous deeper waters were prevalent throughout this time
- Only mid-ramp settings were fully oxygenated
- Stability of oxygenation controlled the ecology of Ediacaran metazoan communities

Dynamic redox conditions control late Ediacaran metazoan ecosystems in the Nama Group, Namibia

**Wood, R. A.^{1*}, Poulton, S.W.², Prave, A.R.³, Hoffmann, K-H.⁴, Clarkson, M.O.^{1,†},
Guilbaud, R.², Lyne, J.W.¹, Tostevin, R.⁵, Bowyer, F.¹, Penny, A.M.¹, Curtis, A.¹, and
Kasemann, S.A.⁶**

¹*School of Geosciences, University of Edinburgh, West Mains Road, Edinburgh, EH9 3JW, UK*

²*School of Earth and Environment, University of Leeds, Leeds, LS2 9JT, UK*

³*Department of Earth Sciences, University of St Andrews, St Andrews, KY16 9AL, UK*

⁴*Geological Survey of Namibia, Private Bag 13297, Windhoek, Namibia*

⁵*Department of Earth Sciences, University College London, Gower Street, London, WC1E 6BT, UK*

⁶*Department of Geosciences, University of Bremen, P.O. Box 330 440, 28334 Bremen, Germany*

[†]*Current address: Department of Chemistry, University of Otago, Union Street, Dunedin, 9016, PO Box 56, New Zealand.*

*Correspondence to: Rachel.Wood@ed.ac.uk

ABSTRACT

The first appearance of skeletal metazoans in the late Ediacaran (~550 million years ago; Ma) has been linked to the widespread development of oxygenated oceanic conditions, but a precise spatial and temporal reconstruction of their evolution has not been resolved. Here we consider the evolution of ocean chemistry from ~550 to ~541 Ma across shelf-to-basin transects in the Zaris and Witputs Sub-Basins of the Nama Group, Namibia. New carbon isotope data capture the final stages of the Shuram/Wonoka deep negative C-isotope excursion, and these are complemented with a reconstruction of water column redox dynamics utilizing Fe-S-C systematics and the distribution of skeletal and soft-bodied metazoans. Combined, these inter-basinal datasets provide insight into the potential role of ocean redox chemistry during this pivotal interval of major biological innovation.

The strongly negative $\delta^{13}\text{C}$ values in the lower parts of the sections reflect both a secular, global change in the C-isotopic composition of Ediacaran seawater, as well as the influence of 'local' basinal effects as shown by the most negative $\delta^{13}\text{C}$ values occurring in the transition from distal to proximal ramp settings. Critical, though, is that the transition to positive $\delta^{13}\text{C}$ values postdates the appearance of calcified metazoans, indicating that the onset of biomineralization did not occur under post-excursion conditions.

Significantly, we find that anoxic and ferruginous deeper water column conditions were prevalent during and after the transition to positive $\delta^{13}\text{C}$ that marks the end of the Shuram/Wonoka excursion. Thus, if the C isotope trend reflects the transition to global-scale oxygenation in the aftermath of the oxidation of a large-scale, isotopically light organic carbon pool, it was not sufficient to fully oxygenate the deep ocean.

Both sub-basins reveal highly dynamic redox structures, where shallow, inner ramp settings experienced transient oxygenation. Anoxic conditions were caused either by episodic upwelling of deeper anoxic waters or higher rates of productivity. These settings supported short-lived and monospecific skeletal metazoan communities. By contrast, microbial (thrombolite) reefs, found in deeper inner- and mid-ramp settings, supported more biodiverse communities with complex ecologies and large skeletal metazoans. These long-lived reef communities, as well as Ediacaran soft-bodied biotas, are found particularly within transgressive systems, where oxygenation was persistent. We suggest that a mid-ramp position enabled physical ventilation mechanisms for shallow water column oxygenation to operate during flooding and transgressive sea-level rise. Our data support a prominent role for oxygen, and for stable oxygenated conditions in particular, in controlling both the distribution and ecology of Ediacaran skeletal metazoan communities.

Keywords: Oxygenation; Neoproterozoic; Biomineralisation; Metazoans; Ediacaran; Ecosystems

1. Introduction

The Ediacaran (635-541 Ma) witnessed a profound biological shift from a world with minimal multicellular diversity and evolutionary stasis, to one of new body plans, skeletal types and novel ecologies, culminating in the appearance of modern-style communities by the early Cambrian (Butterfield, 2007; Erwin et al., 2011). Complex, multicellular, body fossils appeared about 575 million years ago (Ma), represented by the soft-bodied Ediacaran biota found initially in deep waters and later in shallow-marine settings (Martin et al., 2000;

Narbonne and Gehling, 2003). Embryos of possible metazoans are known from at least ~600-580 Ma (Xiao et al., 1998), while the first unequivocal calcified metazoans were present by ~550 Ma (Germs, 1972). The subsequent rapid diversification of metazoans with hard parts around the Precambrian-Cambrian boundary (541 Ma) marks a step change in biodiversity, the complexity of marine ecosystems, and in the workings of the global carbon cycle. Metazoans demand oxygen to support aerobic metabolisms and skeletal hard-parts, and so it has been presumed that a rise in oxygen, perhaps incrementally, facilitated the evolution of this complexity (Fike et al., 2006; Canfield et al., 2007, 2008; McFadden et al., 2008; Scott et al., 2008).

Chemical tracers reveal a profound change in major biogeochemical cycles during the Ediacaran, such as the global Shuram/Wonoka deep negative C-isotope excursion (Burns and Matter, 1993). This has variously been interpreted as being due to oxidation of a substantial reservoir of organic carbon dissolved in the deep ocean (Rothman et al., 2003; Fike et al., 2006), to a large flux of methane released from clathrates (Bjerrum and Canfield, 2011), or to diagenetic phenomena (Derry, 2010). The models of Bristow and Kennedy (2008), however, suggest that there were not enough oxidants available for the model proposed by Fike et al. (2006), and thus that the Shuram could not have represented a large scale oxidation event. Indeed, the global response of ocean redox chemistry to rising oxygen levels through this period has been shown to be complex (Fike et al., 2006; Canfield et al., 2008; Johnston et al., 2010, 2012b; 2013; Sperling et al., 2013a), including in South China the presence of metastable zones of euxinic (anoxic and sulfidic) waters impinging on the continental shelf and sandwiched within ferruginous [Fe(II)-enriched] deep waters (Li et al., 2010). Detailed reconstructions of ocean chemistry suggest that a globally anoxic and ferruginous deep ocean

state existed until at least ~580 Ma, and beyond in certain areas (Canfield et al., 2008; Planavsky et al., 2011; Poulton and Canfield, 2011), whereas surface-water oxygenation is thought to be a near-continuous feature throughout the latter half of the Ediacaran (Canfield et al., 2008). Indeed some have argued that pervasive and persistent oxygenation of the deep ocean did not occur until the later Palaeozoic (e.g. Canfield et al., 2008). There is also evidence to suggest that mid-depth euxinia (free-sulphide in the water column) may have been a feature (but possibly temporally restricted) along some continental shelves at certain times in the Neoproterozoic, but these conditions were sparse compared to the preceding Mesoproterozoic (Canfield et al. 2008; Johnston et al., 2010; Li et al., 2010; Sperling et al., 2013a). The evolution of large metazoans and skeletal hardparts during the Ediacaran period was therefore set within the framework of major perturbations to the C, Fe and S cycles (Des Marais et al. 1992; Logan et al. 1995; Rothman et al., 2003; Fike et al., 2006; Canfield et al., 2007) which are all potentially linked to rising oxygen.

Oxygen requirements in metazoans vary widely, and are determined by size, metabolism, mobility, and the presence or absence of a circulatory system (Vaquer-Sunyer and Duarte, 2008). As a result it has been proposed that metazoans may have been limited to small size (<3 mm), thin body plans, and low diversity communities with simple foodwebs by the relatively low levels of oxygen of the Proterozoic, with the explosion of larger and ecologically diverse organisms in the late Ediacaran and Cambrian related, in part, to increasing oxygen levels (e.g. Cloud, 1968; Runnegar, 1982). Experimental work has also shown that the oxygen levels necessary to support small, primitive metazoans such as sponges (Porifera) are far lower (Mills et al., 2014) than those required for large, active, and

ecologically-important animals such as carnivorous predators (Sperling et al., 2013b; Knoll and Sperling, 2014).

In modern marine environments benthic diversity and biomass decreases with bottom-water oxygen levels, as does individual size and abundance until the skeletal macrobenthos is excluded (e.g. Rhoads & Morse 1971). Hypoxia is a major factor in structuring benthic communities: pelagic-benthic coupling is reduced as are other measures of ecological complexity such as community succession. As oxygen levels decrease, large individuals and long-lived equilibrium species are eliminated, and populations shift towards younger individuals, and smaller and short-lived species that possess opportunistic life histories (Diaz and Rosenberg, 1995). The loss of skeletal biota occurs when oxygen drops below ~ 0.10 present atmospheric levels, a threshold therefore postulated to fuel the Cambrian radiation (Rhoads and Morse, 1971). In addition, fluctuating and unpredictable redox conditions are deleterious to some metazoans, so establishing stable oxygenated conditions (Johnson et al., 2012), even if pO_2 remained relatively low, may have been just as important as a rise in absolute pO_2 .

Some suggest, however, that the Ediacaran oxygen transition was a consequence, not a cause, of metazoan diversification, as the pumping activity of poriferans and cnidarians could have augmented the removal of DOC and smaller phytoplankton from the water column, so substantially enhancing its oxygenation (Butterfield, 2009; Lenton et al., 2014). The evolution of Eumetazoa would have shifted oxygen demand to shelf sea sediments and deeper waters, in turn reducing total phosphorus recycling from sediments so reinforcing through positive feedback the shift to a more oxygenated ocean state (Lenton et al., 2014).

These authors argue that this could have facilitated the rise of more mobile and predatory animals.

Such unresolved controversies persist as to the precise role of oxygen in driving metazoan evolution because current records of this interval are limited both spatially and temporally, and without such, a detailed causal understanding of the relationships between anoxia, evolution and carbon cycle processes is not possible.

We focus on the first appearance of calcified metazoans and their ecology, as found in the ~550 to ~541 Ma Nama Group of southern Namibia, one of the best archives of late Ediacaran Earth history (Germs, 1972; Grotzinger and Miller, 2008). Here, soft-bodied Ediacaran biotas and horizontal burrow systems are found preserved in marine siliciclastic rocks, and abundant calcified metazoans occur in shallow to mid-ramp carbonate settings. This distinctive early calcified biota of stem group Eumetazoa, Cnidaria and Bilateria, or Cnidaria (Wood, 2011) terminates globally at the Precambrian/Cambrian boundary at ~541 Ma (Amthor et al., 2003). A greater diversity of body plans and skeletal organisations, including recognizable stem-group members of extant bilaterian phyla, is subsequently recorded in the first 10 Myr of the Cambrian (Knoll, 2003).

To explore relationships between ocean chemistry, the first appearance of calcified metazoans and their ecology, we present new carbon isotope data across two basin transects that capture the final stages of the Shuram/Wonoka deep negative C-isotope excursion (~550 to ~548 Ma). We then consider Fe-S-C systematics and the distribution of skeletal metazoans across these basins to provide detailed insight into the potential role of ocean redox chemistry during this pivotal interval of major biological innovation. We focus on a suite of clastic and carbonate strata which record coeval sedimentation across a mixed clastic-carbonate ramp

system (Grotzinger et al., 1995). Our samples are from the two basins of the Nama Group, the northern Zaris Basin and southern Witputs Basin, encompassing shallow, inner ramp, through mid-ramp, to deeper, outer-ramp settings (Figure 1). The succession spans the Kuibis Subgroup (~550 to ~547 Ma) in both basins, and the uppermost Schwarzrand Subgroup (~544 to ~541 Ma) in the Witputs Basin, and records the first appearance of calcified metazoans in the fossil record (Germs, 1972), as well as typical late Ediacaran soft-bodied biota. Using these data, in combination with associated sedimentological and palaeobiological observations from our nine sample sites, we have built a spatially resolved redox history that allows exploration of metazoan ecological response to changes in ocean oxygenation.

2. Geological Setting

The Nama Group consists of a variety of fluvial to marine platform carbonate and siliciclastic rocks ranging from upper shoreline/tidal flats to below-wave-base lower shoreface (Grotzinger and Miller, 2008; Saylor et al., 1995, 1998; Germs, 1995) that forms a 3000 m thick foreland basin fill (Gresse and Germs, 1993). The basin is divided by a palaeohigh, the Osis Arch, separating it into the Zaris Sub-Basin in the north and the Witputs Sub-Basin in the south (Figure 1).

The age of the base of the Nama Group is poorly constrained, but is probably between 550-553 Ma (Ries et al., 2010). However, ash beds in the overlying units (Figure 2) provide robust U-Pb zircon age constraints ranging from 548.8 ± 1 Ma in the Hoogland Member of the Kuibis Subgroup (Grotzinger et al., 1995; revised to 547.32 ± 0.31 Ma by Schmitz et al. 2012) to 538.18 ± 1.24 Ma in the upper part of the Schwarzrand Subgroup (Grotzinger et al.,

1995). In the Witputs Sub-Basin the Ediacaran-Cambrian (E-C) boundary is marked by a regionally extensive erosional unconformity (Germs, 1983; Saylor and Grotzinger, 1996; Narbonne et al., 1997; Grotzinger et al., 1995) overlain by an incised-valley fill sequence that contains the earliest Cambrian trace fossil *Treptichnus pedum* (Wilson et al., 2012). Therefore, the Nama Group section spans ~10 Myr and extends to beyond the Proterozoic-Cambrian transition (Saylor et al., 1998; Ries et al., 2010).

Each Sub-Basin has its own distinct stratigraphic framework, although key sequence boundaries and systems tracts can be identified in both, with Transgressive Systems Tracts (TSTs) generally being dominated by siliciclastic rocks whereas various carbonate facies distinguish Highstand Systems Tracts (HSTs; Saylor et al., 1995, 1998; Figure 2). In general, the Kuibis Subgroup thins towards and completely disappears over the Osis Ridge (Germs, 1983, 1995). The basal unit in both sub-basins is the siliciclastic Kanies Member that is overlain by variably developed mixed siliciclastic- to carbonate-dominated units (Grotzinger and Miller, 2008; Saylor et al., 1995; 1998; Germs, 1995). In the Zaris Sub-Basin, carbonate units forming 10-20 meter-scale upward-coarsening, mid-inner ramp to shoreface cycles typify the Lower and Upper Omkyk Members, defining units OS1 and OS2 respectively (Figure 2). The overlying Hoogland Members primarily of heterolithic interbeds that record transgressive-regressive depositional successions in mostly mid-inner ramp to middle shoreface settings; these rocks have been placed in a sequence stratigraphic framework based on the recognition of two unconformity-bounded sequences, K1 and K2 (Saylor et al., 1995, 1998; Figure 2).

In the Witputs Sub-Basin, above the Kanies Member is the carbonate-dominated HST of the Mara Member itself overlain by the TST of the Kliphoeck Member, marked by upper-

shoreface to tide-dominated shoreline sandstones (Saylor et al. 1995). The overlying Mooifontein Member is a thin-bedded shallow-marine limestone that exhibits a relatively uniform constant thickness (30–40 m) across the Witputs Sub-Basin but does pinch out near the Osis Ridge. Its top is marked by an unconformity (S1) having deep canyon-like erosional relief that is filled with conglomerate (Saylor et al, 1998).

The Schwarzrand Group in the Witputs Sub-Basin reaches a maximum thickness of 1000 m. Its lower part consists of the mixed mostly shallow marine clastic and carbonate rocks of the Nudaus (which contains Sequence Boundary S2) through Nasep Member of the Urusis Formation (overlain by Sequence Boundary S3) whereas the Huns (overlain by Sequence Boundary S4), Feldschuhhorn and Spitzkopf Members (overlain by Sequence Boundary S5) comprising its middle part are carbonate-dominated, including spectacular pinnacle reefs that initiated on the flooding surface at the top of the Huns Member and then became enveloped within siltstones of the Feldschuhhorn Member. The top of the Schwarzrand Group is defined by an upper conglomeratic unit, the Nomtsas Formation, that infills incised valleys bracketed by ash beds dated at 542.68 ± 1.245 Ma and 540.61 ± 0.67 Ma (U-Pb zircon; Grotzinger et al., 1995) (Figure 2).

The Nama Group yields various metazoan assemblages. Large (up to 30 cm) horizontal burrow systems with spirite suggesting formation by bilaterian organisms have been found in the siltstones of the Omkyk Member in the Zaris Sub-Basin, 100 m below an ash bed dated at 547.32 ± 0.7 Ma (Macdonald et al., 2014). Burrows are also known from the Huns, Nomtsas and Nasep Members and appear in abundance in the Spitzkopf Member in the Witputs Sub-Basin some 60m below the Ediacaran–Cambrian unconformity (Jensen et al., 2000). Ediacaran fossils such as *Ernietta*, *Pteridinium*, *Swartpuntia*, and *Rangea* (e.g. Narbonne et

al., 1997), vendotaenids (Germis et al., 1986), and the calcified metazoans *Cloudina* spp. (Germis, 1983; Grant, 1990), *Namacalathus* (Grotzinger et al., 2000), and locally *Namapoikia* (Wood et al., 2002), have been described from both the Zaris and Witputs Basins. The oldest Ediacara-type fossils occur in the Mara Member in the Witputs Sub-Basin (Saylor et al., 1995), and the youngest, including *Swartpuntia*, are found in the Spitzkop Member some 60m below the Ediacaran–Cambrian unconformity in the more southerly portion of the Witputs Sub-Basin (Narbonne et al., 1997). The oldest reported *Cloudina* is from the carbonate-dominated Mara Member in the Witputs Basin (Germis 1983). All calcified metazoans occur in either shallow marine carbonate (limestone and dolomite) facies, and may be present along bedding planes of mudstones or dolostones, in thin to thickly bedded packstones and grainstones, or associated with thrombolite reefs.

3. Methods

Nine sections have been studied (see Supplementary Information Table S1 for coordinates), from shallow, inner ramp, through mid-ramp, to deeper, outer-ramp settings (Figure 1). Sections were logged for metazoan occurrence and sampled within the sequence stratigraphic framework of Saylor et al. (1995, 1998) as established by Grotzinger et al. (2005) and Hall et al. (2013)(Figure 2) which allows for consideration of redox dynamics with changes in relative sea-level through time within shelf to basin transects. Samples were chosen that were devoid of mineralised veins or other visible alteration. All weathered surfaces were removed, and the whole rock was either pulverised to a fine powder or sub-sampled via manual excavation for geochemical analysis.

3.1 Carbon and oxygen isotope analyses

The validity of using carbonate rocks as proxy archives for the $\delta^{13}\text{C}$ composition of ancient seawater requires an assessment that geochemical data are representative of primary ocean chemistry. While the Nama Group carbonates have undergone pervasive recrystallization, as well as localised early dolomitization, samples generally show high quality preservation. For example, analysed samples from Zebra River show low Mn/Sr ratios from partial leaches (97% of samples <1), and high [Sr] (294–5802 ppm; with an average of 1509 ± 986 ppm; 40% of samples >1500 ppm) (Figure 3A), and relatively heavy $\delta^{18}\text{O}$ values (89% of samples $>-10\text{‰}$) (Figure 3B). There is also no co-variance between FeT vs $\delta^{18}\text{O}$ and Mn/Sr data (Figure 3). For these reasons the isotopic records presented in this study are considered to track the secular trends of contemporary seawater.

Powdered carbonate samples were analysed at 75°C using a Kiel Carbonate III preparation device. The resulting CO_2 was then analysed on a Thermo Electron Delta+ Advantage stable isotope ratio mass spectrometer. The standard deviation ($n = 61$) of a powdered coral laboratory standard (COR1D, $\delta^{13}\text{C} = -0.648$, $\delta^{18}\text{O} = -4.923$) run on the same days as the study samples was $\pm 0.04\text{‰}$ for $\delta^{13}\text{C}$ and $\pm 0.07\text{‰}$ for $\delta^{18}\text{O}$. All isotopic values are quoted relative to VPDB.

3.2 Total organic C (TOC)

Total organic C (TOC) was measured on an EA mass spectrometer after carbonate removal (two? 10% HCl washes for 48 hours). Excess acid was evaporated and samples dried at 70°C. The reproducibility of 13 internal standards run on the same day as samples was 1.1%.

3.3 Fe-speciation

Fe-speciation is a widely utilized proxy for identifying the regional nature of water column redox conditions. The technique allows identification of oxic and anoxic water column conditions (Raiswell and Canfield, 1998; Poulton and Raiswell, 2002; Poulton and Canfield, 2011), where anoxia may be separated into euxinic (H₂S-bearing) and ferruginous (Fe(II)-containing) (Poulton et al., 2004a). However, the technique lacks the sensitivity to more precisely identify changes in the extent of ocean oxygenation (i.e. where the water column was fully oxic or dysoxic). The proxy gives a measure of highly reactive Fe to total Fe (Fe_{HR}/Fe_T). Fe_{HR} refers to Fe minerals that are considered highly reactive towards biological and abiological reduction under anoxic conditions (Canfield et al., 1992; Poulton et al., 2004b), and includes carbonate-associated Fe (Fe_{carb} ; e.g., ankerite and siderite), ferric (oxyhydr)oxides (Fe_{ox} ; e.g., goethite and hematite), magnetite Fe (Fe_{mag}) and Fe sulfide minerals (Fe_{py} ; e.g., mackinawite and pyrite) (Poulton and Canfield, 2005). Sediments may be enriched in Fe_{HR} under anoxic marine conditions due to either the export of remobilized $Fe_{(aq)}$ from the oxic shelf (Anderson and Raiswell, 2004; Severmann et al., 2008) or under more widespread anoxia, due to upwelling of deep water Fe(II) (Poulton and Canfield, 2011). Precipitation of this mobilized water column Fe is then potentially induced through a variety

of processes, for example through Fe sulfide (pyrite) formation under euxinic conditions (Canfield et al., 1996; Raiswell and Canfield, 1998), or through precipitation of oxidized or partially oxidized Fe minerals under ferruginous conditions (e.g., Zegeye et al., 2012). These processes have the consequence that Fe_{HR}/Fe_T ratios provide a particularly sensitive means to determine whether a depositional setting was oxic or anoxic. Calibration in modern and ancient marine environments suggests that $Fe_{HR}/Fe_T < 0.22$ provides a robust indication of oxic conditions, while $Fe_{HR}/Fe_T > 0.38$ suggests deposition from an anoxic water column (Poulton and Canfield, 2011; Raiswell and Canfield, 1998; Poulton and Raiswell, 2002). Values between 0.22-0.38, however, are somewhat equivocal, and care needs to be taken to determine if such values are a consequence of masking of the additional anoxic water column flux of Fe_{HR} , either due to rapid sedimentation (Raiswell and Canfield, 1998; Poulton et al., 2004a) or due to post-depositional transformation of unsulfidized Fe_{HR} minerals to less reactive sheet silicate minerals (Cumming et al., 2013; Poulton and Raiswell, 2002; Poulton et al., 2010). Additional examination of the Fe_{py}/Fe_{HR} ratio has the unique advantage in that it allows the separation of anoxic settings into euxinic (sulfidic) environments ($Fe_{py}/Fe_{HR} > 0.7-0.8$) and non-sulfidic (Fe-rich; ferruginous) environments ($Fe_{py}/Fe_{HR} < 0.7$) (Poulton and Canfield, 2011; Poulton et al., 2004a).

Fe-speciation extractions were performed according to calibrated extraction procedures (Poulton and Canfield, 2005), whereby Fe_{Carb} was extracted with Na-acetate at pH 4.5 and 50°C for 48 h, Fe_{Ox} was extracted via Na-dithionite at pH 4.8 for 2 h, and Fe_{Mag} was extracted with ammonium oxalate for 6 h. Total Fe (Fe_T) extractions were performed on ashed samples (8 h at 550°C) using HNO_3 -HF- $HClO_4$. Boric acid was used to prevent the formation of Al complexes, allowing total Al to be determined on the same extractions. All Fe concentrations

were measured via atomic absorption spectrometry and replicate extractions gave a RSD of <5% for all steps. Pyrite Fe was determined stoichiometrically by weight from precipitated Ag_2S after chromous chloride distillation (Canfield et al., 1986).

In turbidite settings, high sedimentation rates can cause a dilution of Fe_{HR} (Raiswell and Canfield, 1998; Poulton et al., 2004b) and thus decrease the $\text{Fe}_{\text{HR}}/\text{Fe}_{\text{T}}$ ratio of sediments deposited under an anoxic water column, giving a falsely oxic signal. However, none of the clastic samples measured for Fe_{HR} are from strata that show evidence of turbiditic deposition. Some of the sandstone units in the Spitzkof Member may have been rapidly emplaced, but our analyses are restricted to shales and siltstones in these sections. At Omkyk, the lower part of the succession is dominated by carbonate turbidites, slumps and storm-beds, but all of these units yield an unequivocal anoxic signal. Conversely, preferential trapping of Fe_{HR} in inner shore or shallow marine environments, such as floodplains, salt marshes, deltas and lagoons, can create local $\text{Fe}_{\text{HR}}/\text{Fe}_{\text{T}}$ enrichments (Poulton and Raiswell, 2002). Although the shallow ramp settings of the Nama Group were influenced by fluvial input and experienced intermittent restriction, such Fe_{HR} enrichment is not expected in the normal fully marine settings of the samples analysed.

3.4 Fe-speciation in carbonates

To date, the Fe-speciation technique has been widely applied to shales and mudrocks, for which it was originally calibrated, and the technique has also been successfully applied to some carbonate-rich sediments (e.g., März et al., 2008; Kendall et al., 2012). Indeed, Clarkson et al. (2014) recently demonstrated the utility of Fe-speciation for application to

appropriate carbonate-rich strata. The primary concerns for the use of Fe-speciation in carbonate-rich sediments are related to the decreased detrital components, and hence low Fe_{HR} and Fe_T . This can increase the sensitivity of the proxy to Fe_{HR} inputs that are unrelated to the anoxic water column formation of Fe_{HR} minerals, as might occur during early diagenesis. The impact of this process has been demonstrated to potentially be significant when Fe_T is <0.5 wt% (Clarkson et al., 2014). At $Fe_T >0.5$ wt%, carbonate-rich sediments may behave in a manner which is consistent with shales, generally allowing Fe-speciation and Fe/Al to be used as water column redox proxies for carbonate-rich sediments that have not been subject to Fe_{HR} enrichments during deep burial dolomitization. Thus, samples with $Fe_T <0.5$ wt% have not been used to identify water column redox in the present study. Furthermore, there is no petrographic evidence for deep burial dolomitization in our limestone or dolostone samples, nor has this been documented in other studies (Grotzinger and Miller, 2008; Ries et al., 2010). Early stage dolomitization does not generally cause an increase in Fe_T due to the lack of Fe-rich dolomitizing fluids in shallow burial environments (Clarkson et al., 2014).

These constraints for the application of Fe speciation to carbonates are summarised in Table 1. Clarkson et al. (2014) additionally suggest that carbonate-rich rocks containing <0.5 wt% Fe_T and <0.5 wt% TOC may indicate oxic depositional conditions (Table 1), particularly when both parameters are very low. We apply this approach with caution in the present study, but also, wherever possible, we support this approach by considering the presence of bioturbation to provide independent evidence for oxic water column deposition. It is important to note that wherever possible we sampled shales, siltstones, limestones and dolomites, often within single depositional high-frequency cycles. Therefore, we are able to

consider data from siliciclastic horizons alongside data for carbonates. All $Fe_T > 0.5$ wt% carbonates behave consistently with shales and siltstones (Figures 4 and 5), except where shales have suffered from late stage transformation of unsulfidized highly reactive Fe phases to poorly reactive Fe-rich clays, such that Fe-speciation data can be applied to accurately identify anoxic depositional settings in carbonates providing additional strong support for the validity of our approach. Thus, the carbonate analyses accurately capture the redox chemistry of the ocean during deposition of these sediments.

3.5 Oxidative weathering

Outcrop samples in Namibia have potentially been affected by oxidative weathering. Many shale samples are olive grey with no evidence of Fe oxide staining, suggesting minimal oxidation, but some shale, siltstone and anoxic limestone samples show a pervasive red coloration that might suggest oxidative weathering. Such a coloration might, however, be expected for limestones deposited under ferruginous conditions. We nevertheless consider the possibility for oxidation in more detail. Firstly, it should be noted that pyrite and Fe_{carb} minerals, such as siderite, are the dominant Fe_{HR} minerals that may undergo oxidation. In both cases, however, oxidation will not significantly impact Fe_{HR}/Fe_T or Fe/Al ratios, and hence any interpretation of anoxia remains robust. Oxidation of siderite would transfer Fe_{carb} to the Fe_{ox} pool, and hence this would not affect identification of a ferruginous or euxinic signal. A robust euxinic signature is identified by Fe_{py}/Fe_{HR} ratios > 0.8 (Anderson and Raiswell, 2004; Poulton and Canfield, 2011; Poulton et al., 2004). If we consider an extreme and highly unlikely scenario, whereby there was no Fe_{ox} in the primary sample, and all Fe_{py}

has been oxidized to Fe_{ox} , with no oxidation of Fe_{carb} to Fe_{ox} , approximately 10% of the anoxic samples would give a euxinic signal. However, significant Fe_{carb} (i.e. > 20% of the Fe_{HR} fraction) occurs in ~ 57% of the anoxic samples, indicating that the rocks have not been completely weathered, and hence this extreme scenario is unlikely.

3.6 Fe/Al ratios

Calibration studies suggest that when Fe/Al in siliciclastics is greater than the Phanerozoic average of 0.53 ± 0.11 (Raiswell et al., 2008) these samples are likely to be anoxic. Similarly, Clarkson et al. (2014) derived a normal oxic Fe/Al ratio of 0.55 ± 0.11 for modern sediments, independent of carbonate content. The Fe/Al ratio normalises the Fe_T abundance in order to consider Fe-enrichments independent of background (clastic) supply, and the ratio can be used in tandem with Fe-speciation to better understand Fe systematics. Thus, Fe/Al ratios above ~0.66 provide a robust indication of anoxic water column conditions during deposition.

4 Results

4.1 Kuibis Subgroup: Zaris Basin

Saylor et al. (1995, 1998) have shown that these units were deposited in settings that ranged from a shallow, inner ramp environments through to distal, deep ramp environments that everywhere shallowed-up through time.

4.1.1 Inner Ramp

The sampled section at Zwartmodder (Figure 6; Table S2) consists of ~18 m Kanies Member, followed by 22 m Lower Omkyk Member, 75 m Upper Omkyk Member and ~30 m Hoogland Member. The Lower Omkyk is dominated by dolostones at the base, shallowing to mainly limestone laminates, packstones and grainstones towards the top. There are layers of abundant calcified metazoans (*Cloudina hartmannae* and *Namacalathus*) in the Upper Omkyk and Lower Hoogland Members (HST through TST), including minor thrombolites in the former.

Carbon isotopes show an increasing trend from -2.93 to -0.07‰ in the first ~33 m of the section; for the remaining ~88 m values oscillate on a high frequency from 5.66 to 2.34 ‰ (Figure 6).

Both Fe_T and TOC are variable, from 0 to ~2 wt% and 0.04 to 5.66 wt%, respectively (Figure 6). Intervals where Fe_T and TOC are both <0.5% wt are intermittent in the Upper Omkyk Member TST and HST, and Lower Hoogland Member TST, and are interpreted to represent probable oxic horizons. Fe/Al is above 0.66 in 6 of the 9 samples where Fe_T >0.5 wt%. Fe speciation in shales in the Kanies at the base of the section indicates an oxic signature. Limited carbonate samples with Fe_T >0.5 wt% indicate intermittently anoxic ferruginous conditions in the Lower Omkyk Member TST and Upper Omkyk Member TST and HST, and Lower Hoogland Member TST.

The Omkyk Site consists of ~73 m Lower Omkyk Member and ~30 m Upper Omkyk Member. At Omkyk (Figure 7; Table S3) mid-ramp re-sedimented carbonate beds and stormbeds typify the lower part of the succession and then shallows upward to tidally influenced limestone grainstones with limited thrombolites and abundant *Cloudina hartmannae* and

Namacalathus in the upper part. Some shoaling cycles contain evidence for deposition in supra- to inter-tidal conditions, which may have been subjected to exposure and evaporitic conditions. There are horizons of abundant calcified metazoans in the Upper Omkyk Member late TST only.

Carbon isotopes show a general increasing trend throughout the section, from as negative as -4.22, up to -0.20‰ for first 22 m, then for the remainder of the section climbing to 4.80‰ (Figure 7).

Fe_T is highly variable, from 0.02 to 2.66 wt%. Fe/Al is above 0.66 in 15 of the 19 samples where $Fe_T > 0.5$ wt%. Carbonate intervals where Fe_T and TOC are both < 0.5 wt% are intermittent in the Lower and Upper Omkyk Member TST and HST, and are interpreted to represent probable oxic horizons. Fe speciation in carbonates and shales throughout the lower part of the Lower Omkyk Member, and the Upper Omkyk Member indicates anoxic ferruginous conditions. One carbonate sample in the late TST Upper Omkyk Member associated with bioclasts gives an oxic signature from Fe speciation, and another gives an equivocal oxic signature. Anoxic horizons are interbedded with bioclast-bearing horizons.

4.1.2 Mid Ramp

Zebra River consists of ~65 m Lower Omkyk Member, followed by ~100 m Upper Omkyk Member, ~60 m Lower Hoogland Member and ~75 m Upper Hoogland Member (Figure 8; Table S4). The Kanies Member is a meter-scale package of coarse grained, cross-bedded sandstones. The Lower Omkyk Member is dominated by grainstones whereas, through the TST of the Upper Omkyk Member, thrombolite-stromatolite reefs nucleate and form laterally continuous biostrome layers updip (Grotzinger et al., 2005). *Cloudina*

riemkeae, *C. hartmannae*, and *Namacalathus* are found within thrombolite heads and lag beds in inter-reef shales. Towards the top of the Upper Omkyk Member the section shallows into grainstone-dominated facies with subordinate shale horizons, containing thinner, discontinuous, microbial biostromes. Rip-up clasts and hummocky cross-bedding indicate storm-dominated conditions throughout. The Hoogland Member contains storm-dominated laminites and heterolithics, shallowing towards grainstone-dominated facies.

Carbon isotopes show a general increasing trend throughout the section, from -1.75‰ at the base, reaching values as positive as 6.3‰ at 140 m, then for the remainder of the section are stable at around 3‰ (Figure 8).

Fe_T in carbonate rocks is highly variable, from 0.03 to 1.28 wt%, and follows sequence stratigraphic changes with elevated Fe_T at the base of sequences during early TSTs. Carbonate intervals where Fe_T and TOC are both <0.5 wt% are present throughout the Lower Omkyk Member, the late TST of the Upper Omkyk Member, the late TST of the Lower Hoogland Member, and the entire Upper Hoogland Member, and are interpreted to represent probable oxic horizons. Fe speciation on shales and carbonate rocks indicates oxic conditions in the HST of the Upper Omkyk Member, the TST of the Upper Omkyk Member, and the TST of the Lower Hoogland Member, with anoxic ferruginous signatures limited to the early TST of the Upper Omkyk Member, the HST of the Upper Omkyk Member and the TST of the Lower Hoogland Members. At the base of the Upper Omkyk Member, laterally continuous thrombolitic and other carbonate rocks show a ferruginous signature, but inter-reef and post-reef shales give an oxic signature. However, Fe_T/Al ratios in siliciclastics give an anoxic signal, suggesting that the shales have suffered from late stage transformation of

unsulfidized highly reactive Fe phases to poorly reactive Fe-rich clays (e.g., Poulton and Raiswell, 2002; Poulton et al., 2010; Cumming et al., 2013).

At Driedoornvlagte, the succession covers ~ 47 m of Kanies Member, followed by ~ 60 m Lower Omkyk Member and over 380 m Upper Omkyk Member. The Driedoornvlagte reef (Figure 9; Table S5) is a large pinnacle reef complex, 7 km long and over 250 m high, that accumulated in a mid-ramp setting during the TST of the Upper Omkyk, with markedly increased accommodation space associated with a deeper-water setting compared to Zebra River. The reef is predominantly composed of thrombolitic limestones and grainstones, with minor dolomitisation. Calcified metazoan fossils are found throughout the complex, but are particularly abundant towards the top of the section (Unit 3M of Adams et al., 2004). Here, reef-building *Cloudina hartmannae* (up to 8 mm diameter; Penny et al., 2014) and smaller *C. riemkeae* are found, as well as cryptic *C. riemkeae* within thrombolitic reefs (Wood and Curtis, in press). *Namacalathus* occurs intergrown with *C. riemkeae*, as monospecific aggregations, and also grew in crypts (Wood and Curtis, in press). *Namapoikia* is present occupying fissures within thrombolite reefs (Wood et al., 2002).

Carbon isotope values are given in Smith (1998), and show initial negative values of ~ -3.5‰ at the base of the Kanies Member, transitioning to stable positive values in the Upper Omkyk TST of ~2‰ through the main reef unit (Figure 9).

TOC is very low, between 0.03 and 0.07 wt%. Fe_T is also very low, between 0.005 and 0.383 wt%. Both TOC and Fe_T measurements give results that are consistently far less than 0.5 wt% throughout the sampled section, interpreted to indicate probable persistently oxic conditions. No bioturbation has been noted, however, although preservation may not be common in such energetic settings.

4.1.3. Outer Ramp

At Brak, the succession covers ~ 95 m of Kanies Member, followed by ~ 70 m Lower Omkyk Member. The Brak section (Figure 10; Table S6) is dominated by fine-grained dolostones inter-bedded with thin sandstones and shales indicative of deeper, outer ramp conditions, with shallow subtidal grainstones (limestones) present only towards the very top of the section. There are no metazoans or thrombolites present, but limited stromatolite development at approximately 30 m in the Kanies Member.

Carbon isotopes are negative in the Kanies Member (between -7.44‰ and ~-2.0‰), and increase through the Lower Omkyk Member to 2.45‰ (Figure 10).

Fe_T is variable, from 0.05 to ~1.89 wt% in the Kanies Member, and from 0.08 to 0.132 in the limestones of the Lower Omkyk Member. Fe/Al is above 0.66 in all samples where Fe_T > 0.5 wt%. All Fe speciation values in carbonate rocks and shales in the Kanies Member indicate an anoxic ferruginous signature. No unequivocal redox proxy data are available for the Lower Omkyk Member as all Fe_T < 0.5 wt%, but TOC is notably > 0.5 wt%, ranging from 1.22 to 3.39 wt%.

4.1.4 Fe/Al trends across the Zaris Basin

Fe/Al was run for the end-points in the Zaris Basin transect, namely Zwartmodder (inner ramp), Omkyk (deeper inner ramp), and Brak (outer ramp) sections to explore behaviour across shallow to deep marine settings. These data show enrichments in Fe_T/Al in the deeper, Brak Section compared to the shallowest section, Zwartmodder (Figure 11). The significance of this difference was tested using a Kruskal-Wallis test followed by a Dunn's post-test for

multiple comparisons. The Dunn's result showed a significant difference ($p < 0.05$) for Zwartmodder and Brak, but no significant difference between other comparisons.

4.2 Kuibis Subgroup: Witputs Basin

Two sections were the focus of study and sampling in the Witputs Basin, Arasab (Kanies to Moofontein Members) and Grens (Kanies to Aar Members), both of which record inner ramp restricted settings. Also examined were the Pinnacle Reefs at the top of the Huns Member as well as the Spitzkopf Member at Swartpunt that record a shallowing trend from deeper marine coarsening-upward TST siliciclastic beds to limestones interpreted to have formed in a subtidal ramp positions below storm wave base (Grotzinger and Miller, 2008).

4.2.1 Inner Ramp

Arasab consists of ~ 2 m Kanies Member, followed by ~ 30 m Mara Member, ~ 28 m Lower Kliphoek Member, ~ 50 m Upper Kliphoek (Aar) Member, and ~40 m Moofontein Member (Figure 12; Tables S7A and B). The Mara Member consists of limestone, commonly with evaporitic fabrics, interbedded with thin shale layers. The Lower Kliphoek is dominated by sandstone, followed by the interbedded shales and limestones of the upper Kliphoek (Aar) Member. The Mooifontein Member, a thick limestone containing distinct oolite bands, defines the top of the section. *In situ Ernietta* and transported *Pteridinium* and *Rangea* are abundant in nearby localities of the Lower Kliphoek sandstone and Aar Member units (Hall et al., 2013) but none have been observed in the Arasab section.

$\delta^{13}\text{C}$ values are negative in the lower 22 m of the Mara Member, from -6.22‰ to -0.22‰, and then rise to a maximum of +4.45‰ in the Aar Member before steadily converging on ~3‰ in the upper Mooifontein Member (Figure 12).

Fe_T data from shales range from 0.51 to 0.77 wt% and Fe speciation data indicate fully anoxic ferruginous conditions. Carbonate rocks in the Mara, Kliphoek, and Aar Members had $\text{Fe}_\text{T} > 0.5$ wt%, likewise indicating ferruginous conditions. In samples with $\text{Fe}_\text{T} < 0.5$ wt%, TOC is from 0.05 to 0.13 wt%; these samples are from rocks interbedded with anoxic layers in the Mara and Aar Members, and continuously through the Mooifontein Member, and are taken to indicate sporadic short-lived intervals of probable oxic water column conditions although no bioturbation has been noted.

Stratigraphic coverage of the Grens section (Figure 13; Table S8) covers ~ 25 m of the Kanies Member, followed by ~ 110 m Mara Member, ~ 30 m Lower Kliphoek Member, and ~ 30 m Upper Kliphoek (Aar) Member. Conglomerates, sandstones and shales of the Kanies Member are overlain by interbedded limestone and shale, arranged in m-scale shallowing cycles commonly exhibiting evaporitic fabrics of the Mara Member, which is markedly thicker at Grens than at Arasab implying increasing accommodation space with the deepening ramp succession to the south. The Kliphoek Member is composed of limestone with thin layers of sandstone and is overlain by the shale, limestone, and dolo-cemented sandstones of the Aar Member. At 180 m (Figure 13), *in-situ* dense bedding plane assemblages of the Ediacaran fossil *Nemiana* are abundant.

C-isotope data increase gradually from as low as -7.5‰ in the lower Mara to +2.5‰ in the lower Aar Member, where the first positive values occur (Figure 13).

Fe_T data was >0.5 wt% for only 17 of the 50 samples analysed, with Fe_{HR}/Fe_T for these 17 samples indicating anoxic ferruginous conditions. Where Fe_T is <0.5 wt%, TOC is very low, from 0.04 to 0.2 wt%. This is taken as an indication of probable oxic conditions although no bioturbation has been noted, and these horizons are found interbedded with anoxic horizons in the upper Middle and Kliphoek Members.

4.3 Schwarzrand Group: Witputs Basin

4.3.1. Inner to Outer Ramp

At Swartpunt (Figure 14; Table S10), 500 m of the Spitzkopf Member is exposed terminating at the Ediacaran-Cambrian (E-C) unconformity, and consists of mainly inner ramp HST carbonate rocks and mid- to outer ramp TST siliciclastics. The lower carbonate units define m-scale karst-capped cycles that formed in an energetic, inner-ramp position and contain *in situ* *Namacalathus* and other bioclastic material in some beds. Overlying these rocks is a deeper ramp TST succession consisting of coarsening-upward beds typically comprised of a basal green mudstone upward to ripple-laminated and thick-bedded planar-laminated or cross-bedded sandstones containing burrows and soft-bodied Ediacaran fossils including *Swartpuntia* and a bed with *Pteridinium* (Narbonne et al., 1997). Carbonate rocks above this consist of thin-bedded limestones and dolomites with decimetre-scale microbialites (thrombolites), some with a 'leopardskin' texture (patchy dark grey micrite on a light grey background), and thick and thin-bedded limestones with rare flat-pebble and intraclastic breccias deposited in shallow to deeper subtidal ramp settings below storm wave base. These in turn give way to a HST of laminated, flaggy limestones containing small (< 5

mm) *Cloudina riemkeae* and thrombolites. Horizontal burrows are first noted ~60 m below the E-C unconformity.

Carbon isotope compositions show steady values of around 0.5‰, rising to 2‰ at the level of ash beds 1 and 2, then declining to a minimum of almost 0‰ at the base of the TST shales (Figure 14). This value increases to ~ 1.5‰ at the top of the section.

All but two of the Fe_T values from Swartpunt carbonates are < 0.5 wt%, and these also show consistently low TOC throughout, from 0.04 to 0.07 wt% (Figure 14). This is taken to indicate oxic conditions, and is confirmed by the presence of bioturbation in the upper 60 m of the section. TST clastic samples consistently contain $Fe_T > 0.5$ wt%. Fe_{HR}/Fe_T values vary significantly through the section, but all clastics show an oxic signature. By contrast, two HST carbonate samples with $Fe_T > 0.5$ wt% occurring some 55 m and 20 m below the E-C unconformity show $Fe_{HR}/Fe_T > 0.38$, with low Fe_{py}/Fe_{HR} giving an anoxic ferruginous signature. Taken together, these data suggests predominantly oxic conditions at Swartpunt, with fleeting ferruginous episodes in the final HST.

4.3.2 Mid Ramp

The Pinnacle Reefs at Swartkloofberg Farm (Figure 15; Table S9A and B), initiate on the top of the Huns Member (characterised by interfingering carbonate rocks, siltstones and shales) and form bioherms with a synoptic relief of up to 40 m. After termination of reef growth, the reefs were enveloped by ~ 70 m shales of the Feldschuhhorn Member (Saylor et al., 1995) and then ~ 20 m of shales the Spitskopf Member. Above this is the E-C unconformity and incised valley-fill conglomerate of the Nomtsas Formation.

C-isotope data from the Pinnacle reefs show values from \sim 0.6 to 1.7‰ with no discernible trends (Figure 15).

Carbonate rock samples were taken from one of the pinnacle reefs, and the Feldschuhhorn Member and Spitskopf Member shales were sampled nearby. The sampled reef was composed predominantly of microbialite, with some laminar micritic layers. Microbialite textures are predominantly stromatolitic at the base (approximately 0-5 m), with thrombolitic textures appearing at approximately 5 m height, and aggregations of *Namacalathus* (up to 12 mm diameter) becoming more prevalent towards the top of the reef.

Fe_T through the reef carbonates is low, with values of 0.042 to 0.33 wt%, and TOC is very low, from 0.02 to 0.04 wt% (Figure 15). These are taken to indicate probable continuous oxic conditions. No bioturbation has been noted, however, although preservation may not be common in such energetic settings.

The shales of the Feldschuhhorn and Spitskopf Members give Fe_T measurements ranging from 3.45 to 4.93wt%. Fe_{HR}/Fe_T have values of 0.05-0.21, indicating a persistent oxic depositional environment. One sample, close to the base of the section, gives an equivocal Fe_{HR}/Fe_T value of 0.296.

5 Discussion

5.1 Carbon Isotopes

The smooth and consistent variation in $\delta^{13}C$ values throughout the sampled sections parallels $\delta^{13}C$ variations of contemporaneous terminal Neoproterozoic sections (Ries et al., 2010) from China (Condon et al., 2005; Jiang et al., 2003), Australia (Calver, 2000; Calver,

1995) and Oman (Fike et al., 2006), and suggests that the sampled Nama Group sections are a near-primary record of oceanic $\delta^{13}\text{C}$ and that the Nama Sub-Basins were connected to the global ocean during this interval (Saylor et al., 1998; Grotzinger et al., 1995).

The $\delta^{13}\text{C}$ isotope curves show a striking transition in both basins, from negative values in the Lowermost Kuibis Subgroup climbing to positive values by the Upper Omkyk Member in the Zaris Basin, and the coeval Aar Member in the Witputs Basins with persistent values of $\sim+4$ to $+6\text{‰}$ in the Kuibis Subgroup thereafter (Fig. 16A). The oldest sections, which are in the Witputs Basin, show values as negative as -7.2‰ . This climbing trend coincides in the Zaris Basin with a change of $\delta^{13}\text{C}$ from -2 to -8‰ the distal, deeper ramp setting of the Kanies Member to values of $\delta^{13}\text{C}$ from -4.5 to 4‰ during the Lower Omkyk Member shallow settings. In the upper Schwarzrand Subgroup localities values range from $+0.5$ to $\sim 2\text{‰}$ up to the E-C unconformity.

The strongly negative $\delta^{13}\text{C}$ values in the lower parts of the sections are interpreted as recording the recovery from the global Shuram/Wonoka excursion. In the Nama Group, the complete excursion is not preserved owing to the time-transgressive nature of the basal unconformity (Workman et al., 2002). This reflects both a secular, global change in the C-isotopic composition of Ediacaran seawater, as well as the influence of 'local', basinal effects, as shown by the most negative $\delta^{13}\text{C}$ values occurring in the transition from distal to proximal ramp settings (up to -3‰) and, likewise, the most positive values in the most proximal settings (e.g. Zwartmodder with values up to 6.5‰ as compared to the progressively more distal coeval portions of the Omkyk and Brak sections with values of 5.5‰ and 2.5‰ , respectively). Critical, though, is that while the appearance of calcified

metazoans at these sites in both basins postdates the end the positive (rising) $\delta^{13}\text{C}$ excursion (Fig. 16A), calcified metazoans have been noted in older sediments (Mara Formation) in other locations (Germs 1983). This indicates that the onset of biomineralization did not occur under post-excursion conditions.

5.2 Evolution of Redox in the Nama Group

Redox data reveal a highly dynamic record for the Kuibis and upper Schwarzrand Subgroups, with ferruginous anoxia and oxia varying both spatially and temporally (Fig. 16B). There is no evidence for euxinic (anoxic and sulfidic) waters. In the Kuibis Subgroup in both the Zaris and Witputs Basins, proximal, inner ramp sites show intermittent and laterally discontinuous oxia. Ferruginous water column conditions were a prevalent feature throughout deposition in deep and proximal ramp settings, with persistent oxia forming only in mid-ramp settings. Support for this comes from depth trends in Fe/Al (Figure 11), which suggests that deeper basin enrichments are a consequence of progressive water column precipitation and deposition of Fe during upwelling into shallower waters (hence gradually removing Fe(II) from the water column, leading to lower enrichments in the shallower settings). Conversely, during oxygenated periods, Fe remained in the deep basin, reflected by the low Fe_T values of many of the shallow water oxic samples.

In the upper Schwarzrand Subgroup, oxia becomes more persistent, but again is notably only stable in mid-ramp settings, particularly within TSTs. Indeed, proximal, shallow sites still experienced episodic anoxia in late HSTs close to the E-C unconformity (Figs. 14 and 16B).

Significantly, anoxic and ferruginous deeper water column conditions persist after the transition to positive $\delta^{13}\text{C}$ that marks the end of the Shuram/Wonoka excursion (Fig. 16A and B). Thus, if the C isotope trend reflects the transition to global-scale oxygenation in the aftermath of the oxidation of a large-scale, isotopically light organic carbon pool (Rothman et al., 2003; Johnson et al., 2012), then this oxidation event was not sufficient to fully oxygenate the deep ocean.

The redox-stratified water column does not simply track depth-related stratigraphy, as shallow water facies such as grainstones and shallow-marine mudstones may show either oxic or anoxic signatures. Taken together, these observations suggest that upwelling of deeper anoxic, ferruginous waters into shallow waters was a prevalent feature throughout the succession, resulting in progressive precipitation of water column Fe (II) across the shelf and hence lower Fe/Al ratios in the shallowest water sediments. Interesting is that mid-ramp reef settings, particularly those growing in TSTs, show persistent oxia. Such reefs grew elevated into shallow, highly energetic waters away from proximal influence. So although the water depth of carbonate production may have been similar to inner ramp settings, this suggests that a mid-ramp position enabled physical ventilation mechanisms for water column oxygenation to operate during flooding and transgressive sea-level rise (Figure 17A). By contrast shallow settings during HSTs with limited accommodation space experienced only episodic oxygenation (Figure 17B).

In sum, while placing minimum constraints on global atmospheric $p\text{O}_2$ levels from local iron speciation data of marine sediments is problematic, these data show that throughout the Kuibis Subgroup, from ~550 to ~547 Ma, the Zaris and Witputs Basins were often only intermittently oxic in inner ramp shallow settings, persistently oxic in shallow waters in mid-

ramp settings, but persistently anoxic in deep settings. There are some data to suggest that from the latest Schwartzrund Group up to the E-C unconformity (~543 to ~541 Ma), redox conditions may have become more persistently oxygenated in shallow marine settings, but still experienced episodic anoxia in late HSTs.

5.3 Distribution of metazoan ecology

In the Kuibis Subgroup in both the Zaris and Witputs Basins, inner ramp sites show intermittent and laterally discontinuous oxia. Oxic horizons often coincide with in-situ metazoans, including small representatives of the skeletal forms *Cloudina riemkeae*, *C. hartmannae* and *Namacalathus* (Fig. 18G) at Zwartmodder and Omkyk, and the Ediacaran soft-bodied *Nemiana* at Grens. By contrast, mid-ramp settings show longer intervals of constant oxia, where carbonates are expressed as thrombolitic reefs, particularly during the TSTs. These reefs record relatively biodiverse communities of skeletal metazoans, including large reef-building *Cloudina hartmannae* (Penny et al., 2014; Fig. 18E), large *Namacalathus* (Fig. 18C) and large, cryptic *Namapoikia* (Fig. 18D). The deep water, outer ramp setting at Brak (Fig. 10) records persistent anoxia.

The Pinnacle reefs (Fig. 18A) contain abundant in-situ *Namacalathus*, and these show persistent oxia throughout both the reef limestones and the enclosing clastics of the Feldshuhhorn Formation. Oxic conditions persist into the overlying Spitzkopf Member. The stratigraphically youngest site, Swartpunt (Figure 14) within the Spitzkopf Member shows mainly oxia, but two episodes of impersistent anoxia appear high in the section within the late HSTs. Soft-bodied Ediacaran biota and bioturbation is found in the clastic TST, and aggregations of small *Namacalathus* are found at intervals throughout the succession with

small *Cloudina riemkeae* associated with modest thrombolite growth (Fig. 18H), as well as burrows, in the overlying HST.

Noteworthy is that in shallow, proximal settings in both the Kuibis and Schwarzrand Subgroups, horizons stratigraphically below and between those bearing metazoans show evidence for anoxic ferruginous deposition. These samples often occur within flooding events at the base of metre-scale cycles that shallow upwards into sediments that contain small metazoans. Metazoan horizons generally have either oxic Fe_{HR}/Fe_T ratios (<0.38), or very low Fe_T , suggesting minimal Fe enrichment together with very low TOC. Some horizons (e.g. in the Upper Omkyk), however, record an anoxic water column signal (Figures 7 and 18F). Here, metazoan bioclasts are present only within the upper few mm of individual beds, and are particularly abundant on bedding planes, whereas the lower part of the bed is expressed as dark, fine-scale laminae (laminite) devoid of any bioclastic material (Fig. 18F). However, all microsamples from the lower, dark, laminite to the upper bioclast-bearing region of a single bioclastic horizon have high Fe contents (1.17-2.27 wt%), and anoxic Fe speciation signatures (Fig. 18F).

The distribution of calcified metazoans, as well as their ecology, appears to track redox states, with distinctive ecologies forming in proximal shallow settings with highly transient oxia, compared to deeper mid-ramp, settings with persistent oxia. This highly localised distribution of bioclasts within individual beds (Fig. 18F) emphasises the transient nature of oxygenation. This fine-scale intra-bed variation may be the explanation for the presence of a water column signal which is, on average, anoxic when considering bulk Fe-speciation analyses that incorporate a significant portion of time of single-bed samples, as well as the microsamples, even where thin bioclastic horizons are present. This is particularly

noteworthy as the upper bedding plane of some anoxic horizons (Fig. 18F) show clear evidence of small, *in-situ* *Namacalathus* (Fig. 18G). The presence of *in-situ* metazoans does not support the contention that all bioclasts were reworked from oxic condition into anoxic settings. These data do, however, suggest that these metazoans were either adapted to intermediate redox settings or, more likely, that oxic conditions persisted only on very short (ecological) timescales. A similar sedimentary relationship has been illustrated in *Cloudina*-rich shell beds from Paraguay (Warren et al., 2013), suggesting that this highly localised distribution of bioclasts within individual horizons may be typical for Ediacaran skeletal biota that grew in proximal settings, and indeed may be an expression of the transient nature of oxygenation. In these settings, *Namacalathus* and *Cloudina* occur in short-lived but densely-aggregating monospecific communities (Figs. 18G and H) where the size of individuals is often small, <3-5 mm diameter (Figs. 16B, 18G and H).

By contrast, all thrombolitic reefs (Fig. 18A and B), independent of their size and thickness, show very low FeT and TOC, suggestive of persistent oxic conditions. These reefs are often complex communities that include large and relatively diverse *in-situ* skeletal metazoans, including large *Cloudina* (Fig. 18E), *Namacalathus* up to 40 mm diameter (Fig. 18C), and locally *Namapoikia* (Fig 18D), which can reach up to 1 m. Noteworthy is that these reefs are found mainly in TSTs in deeper proximal and mid-ramp settings where accommodation space was high, and likewise *in-situ* soft-bodied Ediacaran biota, such as *Nemiana* (Fig. 18J) are also found in clastic TSTs. By contrast TSTs have variable oxygenation in inner ramp settings, e.g. the Aar Member at Grens is intermittently oxic, but anoxic at Arasab. The Ediacaran-bearing mid- to outer ramp TST of the Spitzkof Member at Swartpunt is persistently oxic.

In summary, we find a similar relationship to modern marine environments where benthic diversity, as well as individual size and abundance, decreases with bottom-water oxygen levels (Rhoads & Morse 1971). While monospecific communities of small, short-lived taxa grew in fleetingly oxic conditions, the most diverse communities of the Nama Group are found in persistently oxic mid-ramp settings (particularly in TSTs) and include large skeletal forms such as the reef crypt-dweller *Namapoikia*, reef-building *Cloudina hartmanne*, and large *Namacalathus*. Soft-bodied Ediacaran metazoans are also restricted to clastic TSTs which record persistent oxygenation in the sampled sections. Of note also is that large (up to 30 cm) horizontal burrow systems with spriete suggesting formation by mobile bilaterian organisms have also been found in the clastic TST in the Omkyk Member (Macdonald et al., 2014). These observations suggest that the persistent oxygenation present in these particular settings promoted large body size, ecological complex and biodiverse communities, and more metabolically-costly feeding strategies.

6 Conclusions

The strongly negative $\delta^{13}\text{C}$ values in the lower parts of the sections reflect both a secular, global change in the C-isotopic composition of Ediacaran seawater, as well as the influence of 'local' basinal effects, as shown by the most negative $\delta^{13}\text{C}$ values occurring in the transition from distal to proximal ramp settings. Critical, though, is that the transition to positive $\delta^{13}\text{C}$ values postdates the appearance of calcified metazoans, indicating that the onset of biomineralization did not occur under post-excursion conditions.

Significantly, anoxic and ferruginous deeper water column conditions persist during and after the positive $\delta^{13}\text{C}$ excursion that marks the end of the Shuram/Wonoka excursion. Thus, if the C isotope trend reflects the transition to global-scale oxygenation in the aftermath of the oxidation of a large-scale, isotopically light organic carbon pool, it was not sufficient to fully oxygenate the deep ocean.

Previous studies have inferred a direct link between the development of stable oxygenated water column conditions and early Metazoan evolution (Canfield et al., 2007; Johnston et al., 2012). Our data build upon this and show that the oxygenation state of shallow waters during the late Ediacaran was, in fact, highly variable. These data reveal the independent redox histories of the two Nama Group basins, demonstrating that oxygenic ventilation of oceans in the late Ediacaran was probably dependent on local basin hydrodynamics. Persistent oxygenation is found preferentially in mid ramp and deeper inner ramp settings, particularly during transgressive system tracts, suggesting that ventilation was provided by high energy flooding events.

This distinctive redox distribution controlled the distribution and ecology of skeletal metazoan communities of the late Ediacaran. Persistent oxygenation - notably present in mid-ramp settings during TSTs - promoted large body size, ecological complex and relatively biodiverse communities, and more metabolically-costly feeding strategies, while shallow settings with impersistent oxygenation supported small, short-lived, monospecific communities. Our data support a prominent role for oxygen, and for stable oxygenated conditions in particular, in the distribution and structuring of early skeletal metazoan ecosystems.

Acknowledgments

RAW, SAK, and ARP acknowledge support from the Royal Society, and the Namibian Geological Survey. MOC acknowledges support from Edinburgh University Principal's Scholarship Fund. MOC and ARP acknowledge support from the International Centre for Carbonate Reservoirs (ICCR). SWP, RG, RT, FB, ARP, and RAW acknowledge support from NERC through the 'Co-evolution of Life and the Planet' scheme (NE/1005978/1). FB acknowledges support from the Laidlaw Hall fund. We are grateful for permission to access localities on many farms, and we thank A. Horn of Omkyk, U. Schulze Neuhoff of Ababis, L. and G. Fourie of Zebra River, C. Husselman of Driedornvlagte, and L. G' Evereet of Arasab and Swartpunt.

REFERENCES CITED

- Adams, E. W., Schroder, S., Grotzinger, J. P., and McCormick, D.S. 2004. Digital Reconstruction and Stratigraphic Evolution of a Microbial-Dominated, Isolated Carbonate Platform (Terminal Proterozoic, Nama Group, Namibia): *Journal of Sedimentary Research*, v. 74, p 479-497.
- Amthor, J. E., Grotzinger, J.P., Schroder, S., Bowring, S.A., Ramezani, J., Martin, M.W., and Matter, A., 2003, Extinction of *Cloudina* and *Namacalathus* at the Precambrian–Cambrian boundary in Oman: *Geology*, v. 31, p. 431–434.
- Anderson, T.F., and Raiswell, R., 2004. Sources and mechanisms for the enrichment of highly reactive iron in euxinic Black Sea sediments. *Am. J. Sci.*, v. 304, p 203–233.

- Bjerrum, C., and Canfield, D. E. 2011. Towards a quantitative understanding of the late Neoproterozoic carbon cycle: Proceedings of the National Academy of Science USA, v. 109, p. 1542-1547.
- Bristow, T.F. and Kennedy, M. J. 2008. Carbon isotope excursions and the oxidant budget of the Ediacaran atmosphere and ocean. *Geology*, v. 36, no. 11, p. 863-866.
- Burns, S. J., and Matter, A. 1993 Carbon isotopic record of the latest Proterozoic from Oman: *Eclogae Geologicae Helvetica*, v. 86, p. 595–607.
- Butterfield, N. J. 2007. Macroevolution and macroecology through deep time: *Palaeontology*, v. 50, p. 41–55.
- Calver, C. R. 1995. Ediacaran isotope stratigraphy of Australia. Ph.D. dissertation, Macquarie University.
- Calver, C.R. 2000. Isotope stratigraphy of the Ediacaran (Neoproterozoic III) of the Adelaide Rift Complex, Australia, and the overprint of water column stratification. *Precambrian Research*, v. 100, 1 p. 121-150.
- Canfield, D.E., Lyons, T.W., and Raiswell, R. 1996. A model for iron deposition to euxinic Black Sea sediments: *American Journal Science* v. 296, p. 818–834.
- Canfield, D.E., Raiswell, R., Westrich, J., Reaves, C. and Berner, R.A., 1986, The use of chromium reduction in the analysis of inorganic sulphur in sediments and shales: *Chemical Geology*, v. 54, p. 149-155.
- Canfield, D. E., Raiswell, R., and Bottrell, S. 1992. The reactivity of sedimentary iron minerals toward sulfide: *American Journal of Science*, v. 292, p. 818–834.
- Canfield, D. E., Lyons, T.W., and Raiswell, R. 1996. A model for iron deposition

- to euxinic Black Sea sediments: *American Journal of Science*, v. 292, p. 818–834.
- Canfield, D. E., Poulton, S. W., and Narbonne, G. M. 2007. Late-Neoproterozoic Deep-Ocean Oxygenation and the Rise of Animal Life: *Science*, v. 315, p. 99-95.
- Canfield, D., Poulton, S. W., Knoll, A. H., Narbonne, G. M., Ross, G., Goldberg, T., and Strauss, H. 2008. Ferruginous Conditions Dominated Later Neoproterozoic Deep-Water Chemistry: *Science*, v. 321, p. 949-953.
- Clarkson, M.O., Poulton, S.W., Guilbaud, R. and Wood, R., 2014. Assessing the utility of Fe/Al and Fe-speciation to record water column redox conditions in carbonate-rich sediments: *Chemical Geology* v. 382, p. 111-122.
- Cloud Jr, P.E. 1968. Atmospheric and hydrospheric evolution on the primitive Earth: *Science*, v. 160, p. 729–736.
- Condon, D., Zhu, M., Bowring, S., Wang, W., Yang, A., and Jin, Y. 2005. U-Pb Ages from the Neoproterozoic Doushantuo Formation, China: *Science*, v. 308, p. 95-98.
- Creveling, J. R, Johnston, D T., Poulton, S. W, Kotrc B, and März. C. 2014, Phosphorus sources for phosphatic Cambrian carbonates: *Geological Society America Bulletin*, v 126, p145–163.
- Cumming, V. M., Poulton, S. W., Rooney, A. D., Selby, D., 2013. Anoxia in the Terrestrial Environment During the Late Mesoproterozoic: *Geology*, v. 41, p. 583-586.
- Derry, L. A. 2010. On the significance of $\delta^{13}\text{C}$ correlations in ancient sediments: *Earth Planetary Science Letters*, v. 296, p 497-501.
- Des Marais, D. J., Strauss, H., Summons, R. E., and Hayes, J. M. 1992. Carbon Isotope Evidence for the Stepwise Oxidation of the Proterozoic Environment: *Nature*, v 359, p. 605-609.

- Diaz, R. J., and Rosenberg, R. 1995. Marine benthic hypoxia: a review of its ecological effects and the behavioural responses of benthic macrofauna: *Oceanography and Marine Biology: an Annual Review*, v. 33, p. 245-303.
- Erwin, D. H., Laflamme, M., Tweedt, S. M., Sperling, E. A., Pisani, D., and Peterson, K.J., 2011. The Cambrian Conundrum: Early Divergence and Later Ecological Success in the Early History of Animals: *Science*, v. 334, p.1091-1097.
- Fike, D. A., Grotzinger, J. P., Pratt, L. M., and Summons, R. E. 2006. Oxidation of the Ediacaran Ocean: *Nature*, v. 444, p. 744-747.
- Germis, G. J., 1972, New shelly fossils from the Nama Group, South-West Africa: *American Journal of Science*, v. 272, p. 752–761.
- Germis, G. J. B., 1974, Nama Group in southwest Africa and its relationship to pan-African geosyncline. *Journal Geology*, v. 82, 3 p. 301-317.
- Germis, G. J. B. 1983. Implications of a sedimentary facies and depositional environmental analysis of the Nama Group in South West Africa/Namibia. Evolution of the DamaraOrogen: Geological Society of South Africa, Special Publication, v. 11, p. 89-114.
- Germis, G. J. B. 1995. The Neoproterozoic of Southwestern Africa, with emphasis on platform stratigraphy and paleontology. *Precambrian Research*, v. 73, 1-4 p. 137-151.
- Goldberg, T., Poulton, S.W. and Strauss, H. 2005. Sulphur and oxygen isotope signatures of late Neoproterozoic to early Cambrian sulphate, Yangtze Platform, China: Diagenetic constraints and seawater evolution: *Precambrian Research*, v. 137, p. 223-241.

- Gresse, P. G., and Germs, G. J. B. 1993. The Nama Foreland Basin: Sedimentation, Major unconformity Bounded Sequences and Multisided Active Margin Advance: *Precambrian Research*, v. 63, p. 247-272.
- Grotzinger, J., Adams, E. W., and Schroeder, S. 2005. Microbial–metazoan reefs of the terminal Proterozoic Nama Group (c. 550–543 Ma), Namibia: *Geological Magazine*, v. 142, p. 499-517.
- Grotzinger, J. P., Bowring, S. A., Saylor, B. Z., and Kaufman, A. J. 1995. Biostratigraphic and Geochronological Constraints on Early Animal Evolution: *Science*, v. 13, p. 229-272.
- Grotzinger, J. P., Fike, D. A., and Fischer, W. W. 2011. Enigmatic origin of the largest-known carbon isotope excursion in Earth's history: *Nature Geoscience*, v. 4, p. 285–292.
- Grotzinger, J.P., and Miller, R. 2008. The Nama Group, in R. Miller, ed., *The Geology of Namibia, Volume 2: Geological Survey of Namibia Special Publication*, p. 13229-13272.
- Grotzinger, J. P., Watters, W. A., and Knoll, A. H. 2000. Calcified metazoans in thrombolite-stromatolite reefs of the terminal Proterozoic Nama Group, Namibia: *Paleobiology* v. 26, p. 334-359.
- Jensen, S., Saylor, B.Z., Gehling, J.G., and Germs, G.J.B., 2000, Complex tracefossils from the terminal Proterozoic of Namibia: *Geology*, v. 28, p. 143–146.
- Jiang, G., Sohl, L.E., and Christie-Blick, N. 2003. Neoproterozoic stratigraphic comparison of the Lesser Himalaya (India) and Yangtze block (south China): Paleogeographic implication: *Geology*, v. 31, p. 917-920.

- Johnston, D. T., Poulton, S. W., Dehler, C., Porter, S., Husson, J., Canfield, D. E., and Knoll, A. H. 2010. An emerging picture of Neoproterozoic ocean chemistry: Insight from the Chuar Group, Grand Canyon, USA: *Earth Planetary Science Letters*, v. 290, p. 64–73.
- Johnston, D. T., Macdonald, F. A., Gill, B. C., Hoffman, P. F., and Schrag, D. P., 2012a, Uncovering the Neoproterozoic Carbon cycle: *Nature*, v. 483, p. 320–323.
- Johnston, D. T., Poulton, S.W., Goldberg, T., Sergeev, V. N, Podkovyrov, V, Vorob'eva, N.G, Bekker, A., and Knoll, A.H., 2012b, Late Ediacaran redox stability and metazoan evolution: *Earth Planetary Science Letters*, v. 335, p. 25-35.
- Johnston D. T, Poulton, S. W, Tosca, N J., O'Brien, T., Halverson, G. P, Schrag, D. P., and Macdonald, F. A. 2013. Searching for an oxygenation event in the fossiliferous Ediacaran of northwestern Canada: *Chemical Geology*, v. 362, p.273-286.
- Hall, M, Kaufman, A.J., Vickers-Richs, P., Ivantsov, A., Trusler, P., Linnemann, U., Hofmann, M., Elliott, D., Cui, H., Fedonkin, M., Hoffmann, K.- H., Wilson, S.A., Schneider, G., and Smith, J. 2013. Stratigraphy, palaeontology and geochemistry of the late Neoproterozoic Aar Member, southwest Namibia: Reflecting environmental controls on Ediacara fossil preservation during the terminal Proterozoic in African Gondwana: *Precambrian Research*, v 238, p. 214– 232
- Kendall, B., Reinhard, C.T., Lyons, T.W., Kaufman, A.J., Poulton, S.W. and Anbar, A.D. 2010. Pervasive oxygenation along late Archaean ocean margins: *Nature Geoscience*, v. 3, p. 647-652.
- Knoll, A. H. 2003. Vestiges of a beginning? Paleontological and geochemical constraints on early animal evolution: *Annales de Paleontologie*, v. 89, p. 205-221.

- Knoll, A. H., and Sperling, E. A. 2014. Oxygen and animals in Earth history: Proceedings of the National Academy of Science USA, v. 111, p. 3907 - 3908.
- Lenton, T. M., Boyle, R. A., Poulton, S. W., Shields-Zhou, G. A., and Butterfield, N. J. 2014. Co-evolution of eukaryotes and ocean oxygenation in the Neoproterozoic era: *Nature Geoscience*, v. 7, p.257-265.
- Li, C., Love, G. D., Lyons, T. W., Fike, D. A., Sessions, A.L., and Chu, X. 2010. A stratified redox model for the Ediacaran Ocean: *Science*, v. 328, p. 80–83.
- Logan, G. A., Hayes, J. M., Hieshima, G. B. and Summons, R. E. 1995. Terminal Proterozoic reorganization of biogeochemical cycles: *Nature*, v. 376, p. 53–56.
- Macdonald, F. A., Pruss, S. B., and Strauss, J. V. 2014. Trace Fossils with Spreiten from the Late Ediacaran Nama Group, Namibia: Complex Feeding Patterns Five Million Years Before The Precambrian–Cambrian Boundary. *Journal of Paleontology*, v. 88, p. 299-308.
- Martin, M. W., Grazhdankin, D. V., Bowring, S. A., Evans, D. A. D, Fedonkin, M. A., and Kirschvink, J. A. 2000. Age of Neoproterozoic Bilaterian Body and Trace Fossils, White Sea, Russia: Implications for Metazoan Evolution: *Science*, v. 288, p. 841-845.
- März, C., Poulton, S.W., Beckmann, B., Kuster, K., Wagner, T. and Kasten, S. 2008. Redox sensitivity of P cycling during marine black shale formation: Dynamics of sulfidic and anoxic non-sulfidic bottom waters: *Geochimica et Cosmochimica Acta*, v. 72, p. 3703-3717.
- Mills, D. B., Ward, L. M., Jones, C., Sweeten, B., Forth, M., Treusch, A. H. and Canfield, D. E. 2014. Oxygen requirements of the earliest animals: Proceedings of the National Academy of Science USA, v. 111, p. 4168–4172.

- Narbonne, G. M., and J. G. Gehling. 2003. Life after Snowball: the oldest complex Ediacaran fossils. *Geology*, v. 31, p. 27–30.
- Narbonne, G.M., Kaufman, A.J., and Knoll, A.H., 1994, Integrated chemostratigraphy and biostratigraphy of the Windermere Supergroup, northwestern Canada: implications for Neoproterozoic correlations and the early evolution of animals. *Geological Society of America bulletin*, v. 106, 10 p. 1281-1292.
- Narbonne, G.M., Saylor, B.Z., and Grotzinger, J.P. 1997. The youngest Ediacaran fossils from Southern Africa: *Journal of Paleontology*, v. 71, 6 p. 953-967.
- Penny, A. M. , Wood R., Curtis, A., Bowyer F., Tostevin, R., Hoffman, K. – H. 2014. Ediacaran metazoan reefs from the Nama group, Namibia. *Science*, v. 344, p. 1504-1506.
- Planavsky, N.J., McGoldrick, P., Scott, C.T., Li, C., Reinhard, C.T., Kelly, A.E., Chu, X., Bekker, A., Love, G.D., and Lyons, T.W., 2011. Widespread iron-rich conditions in the mid-Proterozoic ocean: *Nature* v. 477, p. 448–451.
- Poulton, S.W. and Raiswell, R. 2002. The low-temperature geochemical cycle of iron: From continental fluxes to marine sediment deposition. *American Journal of Science*, v. 302, p. 774-805.
- Poulton, S.W. and Canfield, D.E. 2005. Development of a sequential extraction procedure for iron: implications for iron partitioning in continentally derived particulates: *Chemical Geology*, v. 214, p. 209-221.
- Poulton, S.W., Fralick, P.W. and Canfield, D.E. 2004a. The transition to a sulphidic ocean ~1.84 billion years ago: *Nature*, v. 431, p. 173-177.

- Poulton, S.W, Krom, M. D., and Raiswell, R. 2004b. A revised scheme for the reactivity of iron (oxyhydr)oxide minerals towards dissolved sulfide: *Geochimica et Cosmochimica Acta*, v. 68, p. 3703-3715.
- Poulton, S.W., Fralick, P.W. and Canfield, D.E. 2010. Spatial variability in oceanic redox structure 1.8 billion years ago: *Nature Geoscience*, v. 3, p. 486-490.
- Poulton, S. W., and Canfield, D. E. 2011. Ferruginous conditions: A dominant feature of the ocean through Earth's history: *Elements*, v. 7, p. 107-112.
- Raiswell, R., and Canfield, D.E., 1998. Sources of iron for pyrite formation in marine sediments. *American Journal Science*, v. 298, p. 219–245.
- Raiswell R, *et al.* (2008) Turbidite depositional influences on the diagenesis of Beecher's Trilobite Bed and the Hunsruck Slate; Sites of soft tissue pyritization. *American Journal of Science* 308(2):105-129.
- Rhoads, D. C., and Morse, J. W. 1971. Evolutionary and ecologic significance of oxygen-deficient basins. *Lethaia*, v. 4, p. 413–428.
- Ries, J.B., Fike, D.A., Pratt, L.M., Lyons, T.W., and Grotzinger, J.P. 2010. Super-heavy pyrite ($\delta^{34}\text{S}_{\text{pyr}} > \delta^{34}\text{S}_{\text{SCAS}}$) in the terminal Proterozoic Nama Group, Southern Namibia: A consequence of low seawater sulfate at the dawn of animal life. *Geology*, v. 37, p. 743-746.
- Rothman, D. H., Hayes, J. M., and Summons, R. E. 2003. Dynamics of the Neoproterozoic carbon cycle: *Proceedings of the National Academy of Science USA*, v. 100, p. 8124–8129.

- Runnegar, B. 1982. Oxygen requirements, biology and phylogenetic significance of the late Precambrian worm *Dickinsonia*, and the evolution of the burrowing habit: *Alcheringa*, v. 6, p. 223–239.
- Saylor, B.Z., and Grotzinger, J.P., 1996, Reconstruction of important Proterozoic-Cambrian boundary exposures through the recognition of thrust deformation in the Nama Group of southern Namibia: *Communications of the Geological Survey of Namibia*, v. 11, p. 1-12.
- Saylor, B.Z., Grotzinger, J.P., and Germs, G.J.B. 1995. Sequence stratigraphy and sedimentology of the Neoproterozoic Kuibis and Schwarzrand Subgroups (Nama Group), southwestern Namibia: *Precambrian Research*, v. 73, p. 153-171.
- Saylor, B.Z., Kaufman, A.J., Grotzinger, J.P., and Urban, F., 1998, A composite reference section for terminal Proterozoic strata of southern Namibia: *Journal of Sedimentary Research*, v. 68, 6 p. 1223-1235.
- Schmitz, M. D (2012) Radiogenic Isotope Geochronology *in*: Gradstein, F.M., Ogg, J.G., Schmidt, M.D., and Ogg, G.M. (eds.), *Geologic Time Scale 2012*, Elsevier, p. 115-126.
- Severmann, S., Lyons, T. W., Anbar, A., McManus, J. and Gordon, G. 2008. Modern iron isotope perspective on the benthic iron shuttle and the redox evolution of ancient oceans: *Geology* v. 36, p. 487-490.
- Smith, O.A. 1998. Terminal Proterozoic carbonate platform development: stratigraphy and sedimentology of the Kuibis Subgroup (ca. 550–548 Ma), Northern Nama Basin, Namibia [unpublished M.Sc. thesis]: Cambridge, Massachusetts, Massachusetts Institute of Technology, 132 p.

- Sperling, E. M., Halverson, G. P., Knoll, A. H., Macdonald, F. A., and Johnston, D. T. 2013a. A basin redox transect at the dawn of animal life. *Earth Planetary Science Letters*, v. 371, p. 143–155.
- Sperling, E. A., Freider, C. A., Raman, A. V., Mirguis, P. R., Levin, L. A., and Knoll, A. H. 2013b. Oxygen, ecology and the Cambrian radiation of animals. *Proceedings of the National Academy of Science USA*, v. 110, p. 13446–13451.
- Swart, P. K., and Eberli, G., 2005, The nature of the $d^{13}C$ of periplatform sediments: Implications for stratigraphy and the global carbon cycle: *Sedimentary Geology*, v. 175, p. 115-129.
- Vaquer-Sunyer, R., and Duarte, C.M., 2008. Thresholds of hypoxia for marine biodiversity. *Proceedings of the National Academy of Science USA*, v. 105, p. 15452–15457.
- Warren, L.V, Simões, M. G., Fairchild, T. R., Riccomini, C., Gaucher, C., Anelli, L. E., Freitas, B. T., Boggiani, P. C., and Quaglio, F. 2013. Origin and impact of the oldest metazoan bioclastic sediments: *Geology*, v. 41, p. 507-510.
- Wilson, J. P. et al. 2012. Deep-water incised valley deposits at the Ediacaran-Cambrian boundary in Southern Namibia contain abundant *Treptichnus pedum*. *Palaios*, v. 27, p. 252-273.
- Wood, R. and Curtis, A. in press. Extensive metazoan reefs from the Ediacaran Nama Group, Namibia: the rise of benthic suspension feeding: *Geobiology*
- Wood, R.A., Grotzinger J. P. and Dickson, J.A.D. 2002. Proterozoic modular biomineralized metazoan from the Nama Group: *Science* v 296, p. 2383-2386.
- Wood, R.A. 2011. Paleocology of the earliest skeletal metazoans: implications for early biomineralization: *Earth Sciences Reviews*, v. 106, p. 184–190.

- Workman, R. K., Grotzinger, J. P., and Hart, S. R. 2002. Constraints on Neoproterozoic ocean chemistry from ^{13}C and ^{11}B analyses of carbonates from the Witvlei and Nama Groups, Namibia: *Geochimica Cosmochimica Acta*, v. 66, p. 847.
- Xiao, S., Zhang, Y., and Knoll, A. H. 1998. Three-dimensional preservation of algae and, and and...
- Zegeye, A., Bonneville, S., Benning, L. G., Sturm, A., Fowle, D.A., Jones, C., Canfield, D. E., Ruby, C., MacLean, L. C., Nomosatryo, S., Crowe, S. A., and Poulton, S. W. 2012. Green rust formation controls nutrient availability in a ferruginous water column: *Geology*, v. 40, p. 599-602.
- Zerkle, A. L., Claire, M. W., Domagal-Goldman, S.D., Farquhar, J., and Poulton, S W. 2012. A bistable organic-rich atmosphere on the Neoarchaeon Earth: *Nature Geoscience*, v. 5, p. 359-363.

Tables

Water column Redox	Fe _T (wt%)	TOC (wt%)	Fe _{HR} /Fe _T	Fe/Al
Oxic	>0.5	N/A	<0.22	0.55 ± 0.11
Probably Oxic*	<0.5	<0.5	N/A	N/A
Anoxic	>0.5	NA	>0.38	>0.64

Table 1

Table captions

Table 1: Summary of threshold values for the use of Fe speciation and Fe/Al as palaeo-redox proxies in carbonate-rich sediments that have not experienced Fe addition during deep burial dolomitization. TOC = total organic carbon. NA = not applicable (i.e., no threshold value required). *In the absence of late stage dolomitization or rapid rates of sedimentation. Modified from Clarkson et al., 2014.

Figure Captions

Figure 1: **A**, Simplified map showing the geological setting, subdivisions, and sub-basins of the late Ediacaran to early Cambrian Nama Group of southern Namibia (modified from Grotzinger and Miller, 2008), and sampled Sites: 1, Zwartmodder (Omkyk Farm); 2, Omkyk (Omkyk Farm); 3, Zebra River; 4, Dreidornvlagte; 5, Brak (Ababis Farm); 6, Arasab; 7, Grens; 8, Pinnacle Reefs (Swartkloofberg Farm); 9, Swartpunt. **B**, Relative palaeodepth position of Sites within the northern Zaris and southern Witputs Basins. Depositional interpretations from Saylor et al. (1995, 1998).

Figure 2: Stratigraphy, sequence boundaries, and dated ash beds of the Zaris and Witpus Sub-Basins Nama Group, Namibia (modified from Saylor et al., 1995, 1998; Grotzinger et al., 2005; Hall et al., 2013).

Figure 3. Cross plots of A, Fe_T vs $\delta^{18}O$ and, B, Fe_T vs of Mn/Sr data showing no covariance. Blue = Limestone, red = Dolomite.

Figure 4. Distribution of all Fe-speciation data from the Nama Group. Yellow=clastic; Blue = limestone; red = dolomite.

Figure 5. Fe_{py}/Fe_{HR} against Fe_{HR}/Fe_T to identify ferruginous vs euxinic anoxic conditions in samples with $Fe_T > 0.5$ wt%. Yellow=clastic; Blue = limestone; red = dolomite.

Figure 6. Zwartmodder section: Stratigraphy, lithology, metazoan distribution, $\delta^{13}C$, Fe_T , TOC, Fe speciation and Fe/Al data. Where $Fe_T > 0.5$ wt%, $Fe_{HR}/Fe_T < 0.22$ provides a robust indication of oxic conditions and $Fe_{HR}/Fe_T > 0.38$ suggests deposition from an anoxic water column. Fe_{py}/Fe_{HR} ratio separates anoxic settings into euxinic (sulfidic) environments ($Fe_{py}/Fe_{HR} > 0.7-0.8$) and non-sulfidic (Fe-rich; ferruginous) environments ($Fe_{py}/Fe_{HR} < 0.7$). Fe/Al is used to help interpret Fe_{HR}/Fe_T values between 0.22-0.38; when Fe/Al is greater than 0.66 samples are likely to be anoxic. < 0.5 wt% Fe_T and < 0.5 wt% TOC may indicate oxic depositional conditions, but this requires independent palaeontological evidence.

Figure 7: Omkyk section: Stratigraphy, lithology, metazoan distribution, $\delta^{13}\text{C}$, Fe_T , TOC, Fe speciation and Fe/Al data. Where $\text{Fe}_\text{T} > 0.5$ wt%, $\text{Fe}_\text{HR}/\text{Fe}_\text{T} < 0.22$ provides a robust indication of oxic conditions and $\text{Fe}_\text{HR}/\text{Fe}_\text{T} > 0.38$ suggests deposition from an anoxic water column. $\text{Fe}_\text{py}/\text{Fe}_\text{HR}$ ratio separates anoxic settings into euxinic (sulfidic) environments ($\text{Fe}_\text{py}/\text{Fe}_\text{HR} > 0.7-0.8$) and non-sulfidic (Fe-rich; ferruginous) environments ($\text{Fe}_\text{py}/\text{Fe}_\text{HR} < 0.7$). Fe/Al is used to help interpret $\text{Fe}_\text{HR}/\text{Fe}_\text{T}$ values between 0.22-0.38; when Fe/Al is greater than 0.66 samples are likely to be anoxic. < 0.5 wt% Fe_T and < 0.5 wt% TOC may indicate oxic depositional conditions, but this requires independent palaeontological evidence.

Figure 8: Zebra River section: Stratigraphy, lithology, metazoan distribution, $\delta^{13}\text{C}$, Fe_T , TOC, and Fe speciation. Where $\text{Fe}_\text{T} > 0.5$ wt%, $\text{Fe}_\text{HR}/\text{Fe}_\text{T} < 0.22$ provides a robust indication of oxic conditions and $\text{Fe}_\text{HR}/\text{Fe}_\text{T} > 0.38$ suggests deposition from an anoxic water column. $\text{Fe}_\text{py}/\text{Fe}_\text{HR}$ ratio separates anoxic settings into euxinic (sulfidic) environments ($\text{Fe}_\text{py}/\text{Fe}_\text{HR} > 0.7-0.8$) and non-sulfidic (Fe-rich; ferruginous) environments ($\text{Fe}_\text{py}/\text{Fe}_\text{HR} < 0.7$). Fe/Al is used to help interpret $\text{Fe}_\text{HR}/\text{Fe}_\text{T}$ values between 0.22-0.38; when Fe/Al is greater than 0.66 samples are likely to be anoxic. < 0.5 wt% Fe_T and < 0.5 wt% TOC may indicate oxic depositional conditions, but this requires independent palaeontological evidence.

Figure 9: Driedornvlagte section: Stratigraphy, lithology and $\delta^{13}\text{C}$ (modified from Smith, 1998), metazoan distribution, Fe_T , and TOC. < 0.5 wt% Fe_T and < 0.5 wt% TOC may indicate oxic depositional conditions, but this requires independent palaeontological evidence.

Figure 10: Brak section: Stratigraphy, lithology, $\delta^{13}\text{C}$, Fe_T , TOC, Fe speciation and Fe/Al data. Where $\text{Fe}_\text{T} > 0.5 \text{ wt}\%$, $\text{Fe}_\text{HR}/\text{Fe}_\text{T} < 0.22$ provides a robust indication of oxic conditions and $\text{Fe}_\text{HR}/\text{Fe}_\text{T} > 0.38$ suggests deposition from an anoxic water column. $\text{Fe}_\text{py}/\text{Fe}_\text{HR}$ ratio separates anoxic settings into euxinic (sulfidic) environments ($\text{Fe}_\text{py}/\text{Fe}_\text{HR} > 0.7-0.8$) and non-sulfidic (Fe-rich; ferruginous) environments ($\text{Fe}_\text{py}/\text{Fe}_\text{HR} < 0.7$). Fe/Al is used to help interpret $\text{Fe}_\text{HR}/\text{Fe}_\text{T}$ values between 0.22-0.38; Fe/Al is used to help interpret $\text{Fe}_\text{HR}/\text{Fe}_\text{T}$ values between 0.22-0.38; when Fe/Al is greater than 0.66 samples are likely to be anoxic. $< 0.5 \text{ wt}\% \text{ Fe}_\text{T}$ and $< 0.5 \text{ wt}\% \text{ TOC}$ may indicate oxic depositional conditions, but this requires independent palaeontological evidence.

Figure 11: Fe/Al trends across the Zaris Basin, in a column scatter plot for three studied Zaris Basin Sites, showing frequency distribution of the data. Data are offset horizontally to avoid overlap, and horizontal line marks median value. All 3 sites have a non-Gaussian but similar shaped distribution allowing comparison of medians using a Kruskal-Wallis test. The plotted lines are the median values of Fe/Al = 1.52 for Brak), 1.12 for Omkyk, and Fe/Al = 0.71 for Zwartmodder. P value = 0.003.

Figure 12: Arasab section: Stratigraphy, lithology, $\delta^{13}\text{C}$, Fe_T , TOC, and Fe speciation. Where $\text{Fe}_\text{T} > 0.5 \text{ wt}\%$, $\text{Fe}_\text{HR}/\text{Fe}_\text{T} < 0.22$ provides a robust indication of oxic conditions and $\text{Fe}_\text{HR}/\text{Fe}_\text{T} > 0.38$ suggests deposition from an anoxic water column. $\text{Fe}_\text{py}/\text{Fe}_\text{HR}$ ratio separates anoxic settings into euxinic (sulfidic) environments ($\text{Fe}_\text{py}/\text{Fe}_\text{HR} > 0.7-0.8$) and non-sulfidic (Fe-rich; ferruginous) environments ($\text{Fe}_\text{py}/\text{Fe}_\text{HR} < 0.7$). $< 0.5 \text{ wt}\% \text{ Fe}_\text{T}$ and $< 0.5 \text{ wt}\% \text{ TOC}$ may indicate oxic depositional conditions, but this requires independent palaeontological evidence.

Figure 13: Grens section: Stratigraphy, lithology, metazoan distribution, $\delta^{13}\text{C}$, Fe_T , TOC, and Fe speciation. Where $\text{Fe}_\text{T} > 0.5$ wt%, $\text{Fe}_\text{HR}/\text{Fe}_\text{T} < 0.22$ provides a robust indication of oxic conditions and $\text{Fe}_\text{HR}/\text{Fe}_\text{T} > 0.38$ suggests deposition from an anoxic water column. $\text{Fe}_\text{py}/\text{Fe}_\text{HR}$ ratio separates anoxic settings into euxinic (sulfidic) environments ($\text{Fe}_\text{py}/\text{Fe}_\text{HR} > 0.7-0.8$) and non-sulfidic (Fe-rich; ferruginous) environments ($\text{Fe}_\text{py}/\text{Fe}_\text{HR} < 0.7$). < 0.5 wt% Fe_T and < 0.5 wt% TOC may indicate oxic depositional conditions, but this requires independent palaeontological evidence.

Figure 14: Swartpunt section: Stratigraphy, lithology, metazoan distribution, $\delta^{13}\text{C}$, Fe_T , TOC, and Fe speciation. Where $\text{Fe}_\text{T} > 0.5$ wt%, $\text{Fe}_\text{HR}/\text{Fe}_\text{T} < 0.22$ provides a robust indication of oxic conditions and $\text{Fe}_\text{HR}/\text{Fe}_\text{T} > 0.38$ suggests deposition from an anoxic water column. $\text{Fe}_\text{py}/\text{Fe}_\text{HR}$ ratio separates anoxic settings into euxinic (sulfidic) environments ($\text{Fe}_\text{py}/\text{Fe}_\text{HR} > 0.7-0.8$) and non-sulfidic (Fe-rich; ferruginous) environments ($\text{Fe}_\text{py}/\text{Fe}_\text{HR} < 0.7$). < 0.5 wt% Fe_T and < 0.5 wt% TOC may indicate oxic depositional conditions, but this requires independent palaeontological evidence.

Figure 15: Pinnacle Reefs section: Stratigraphy, lithology, metazoan distribution, $\delta^{13}\text{C}$, Fe_T , and TOC. < 0.5 wt% Fe_T and < 0.5 wt% TOC may indicate oxic depositional conditions, but this requires independent palaeontological evidence.

Figure 16. A, Carbon isotopes, stratigraphy and inferred general water depth settings for nine Sites that transect the Zaris and Witputs Basin, Nama Group, Namibia. **B,** Redox dynamics

based on Fe_{HR}/Fe_T , Fe/Al , and Fe_P/Fe_{HR} profiles, and calcified metazoan occurrence and ecology.

Figure 17: Inferred general redox structure for the Nama Group, Namibia, based on Fe-speciation and Fe/Al . A, Transgressive Systems Tract, B, Highstand Systems Tract. Facies distribution based on the Kuibis Formation, after Saylor et al., 1995.

Figure 18: Metazoan response to persistence of oxygenation. *Persistent oxygenation:* A, Reefs; B, Thrombolites (microbialites); C, Thrombolite-associated *Namacalathus* (20-40 mm); D, *Namapoikia* (cryptic); E, Reef-building *Cloudina hartmanne* (5-8 mm). *Impersistent oxygenation:* F, Vertical polished section through individual bioclastic horizon (*Namacalathus*) showing lower laminated lithology, with surficial upper bioclastic horizon, and attendant Fe_T and Fe speciation data. G, Aggregating, bedding plane showing in-situ monospecific assemblage of *Namacalathus* (< 5 mm) with evidence of distortion due to close-packing during growth (arrowed); H, *Cloudina* (< 3 mm) attached to low relief thrombolite. J, *In-situ* aggregating *Nemiana*.

Figure 1

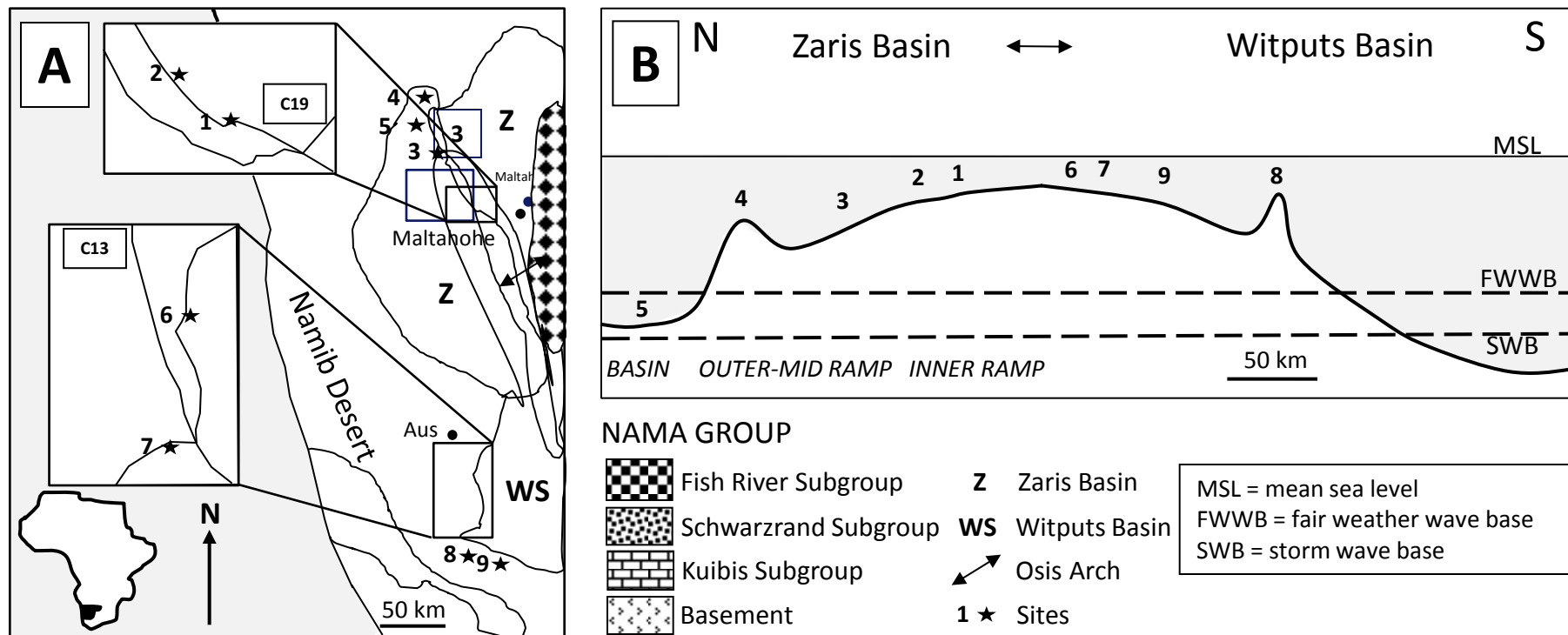


Figure 2

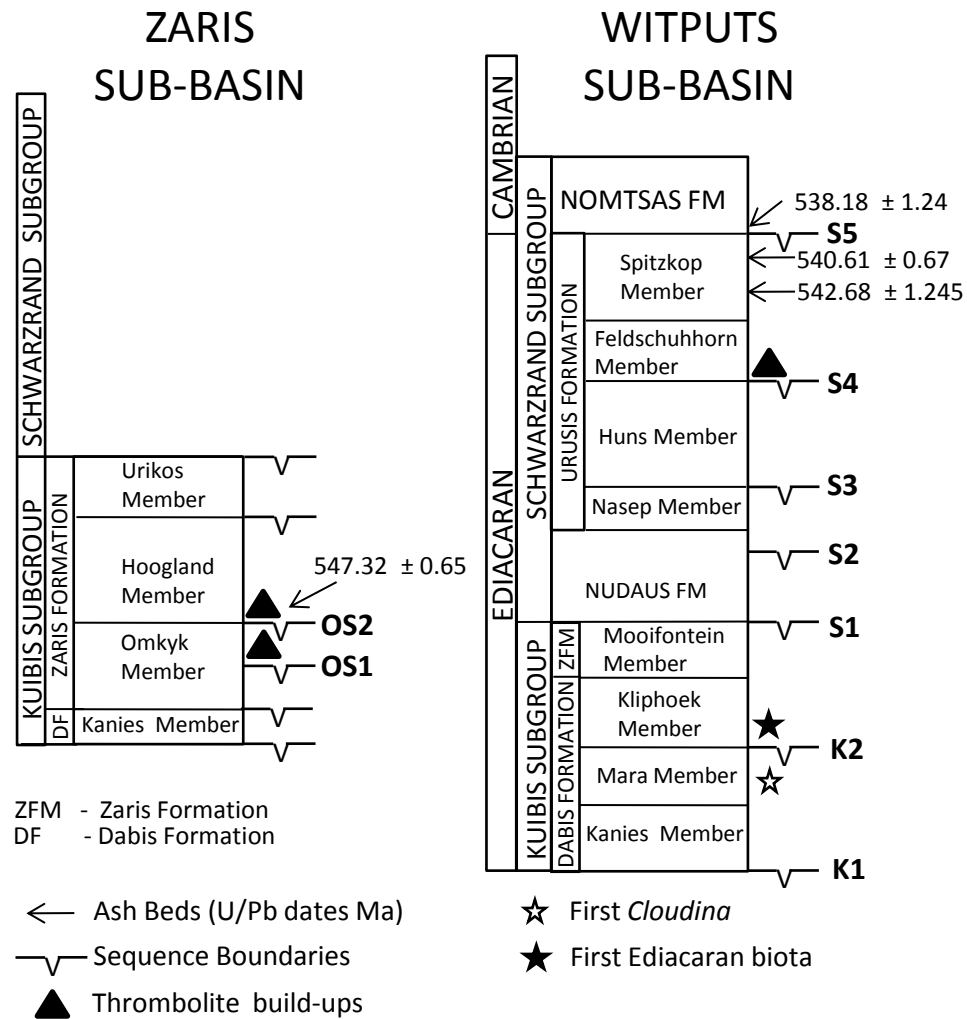


Figure 2

Figure 3

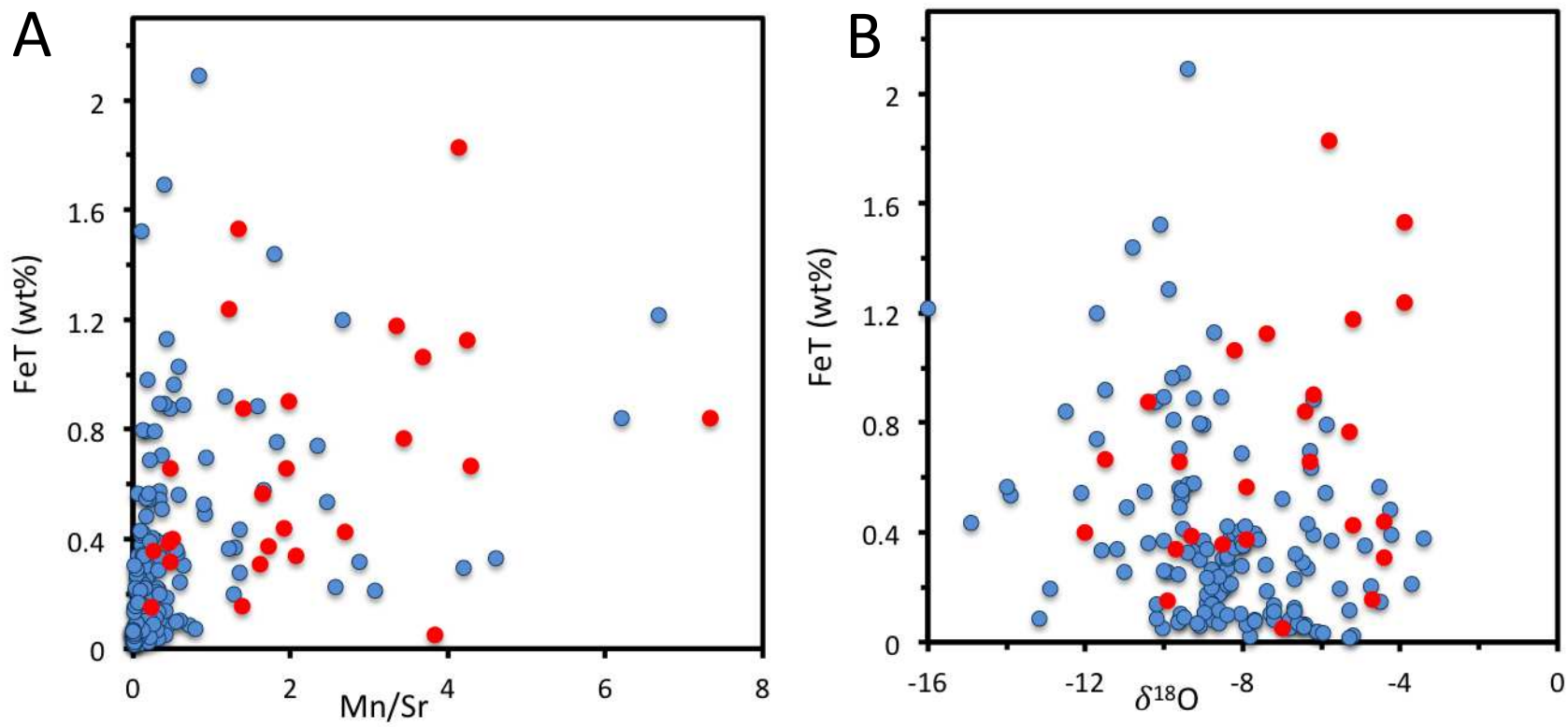


Figure 3

Figure 4

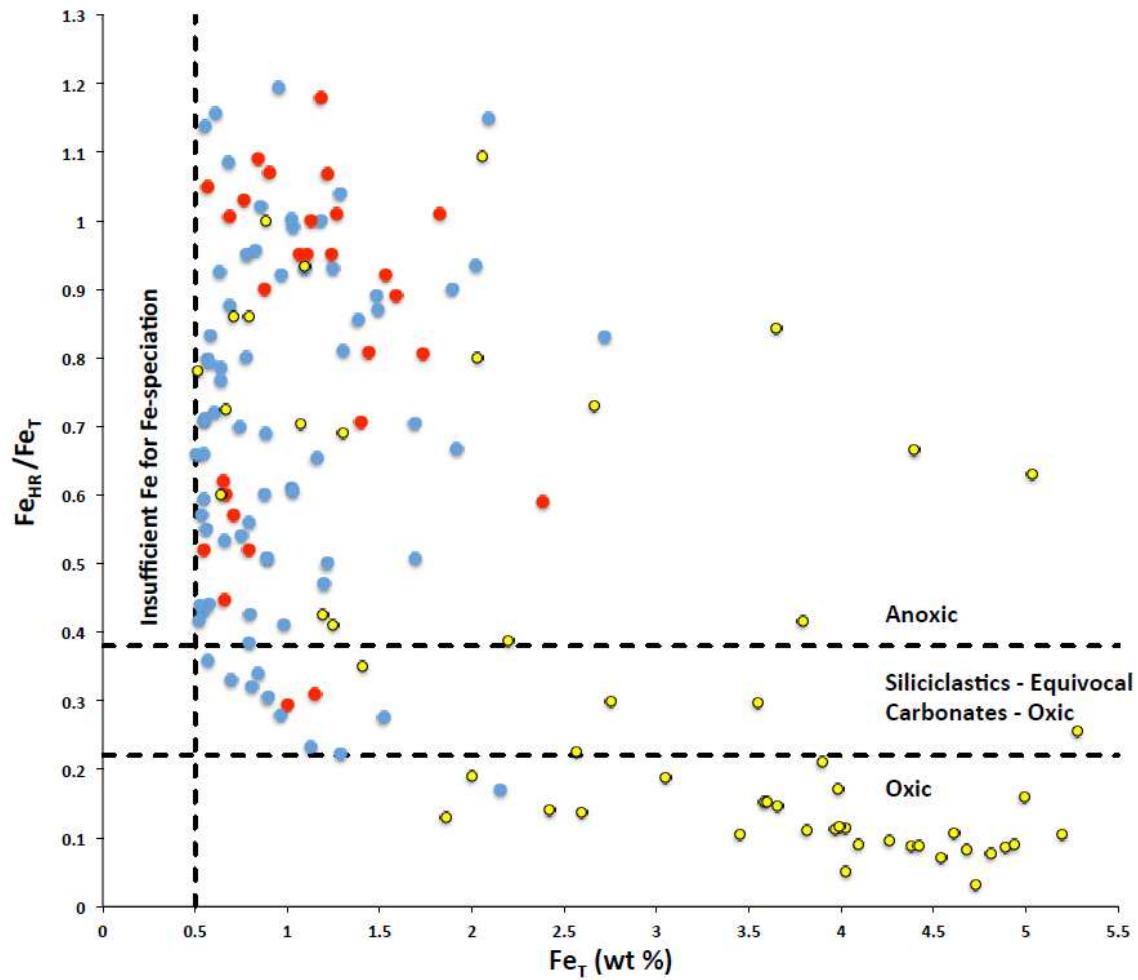


Figure 4

Figure 5

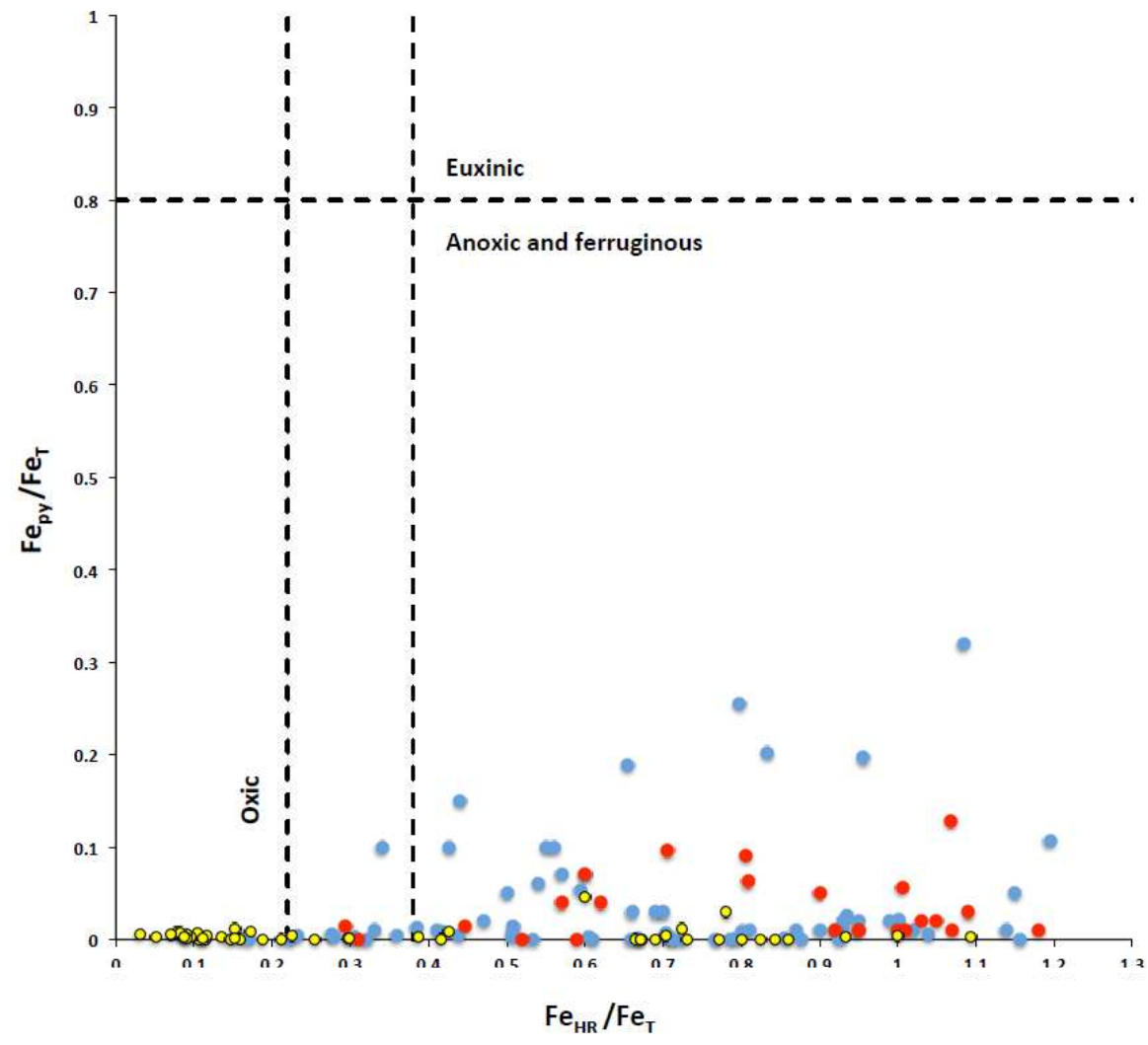


Figure 5

Figure 6

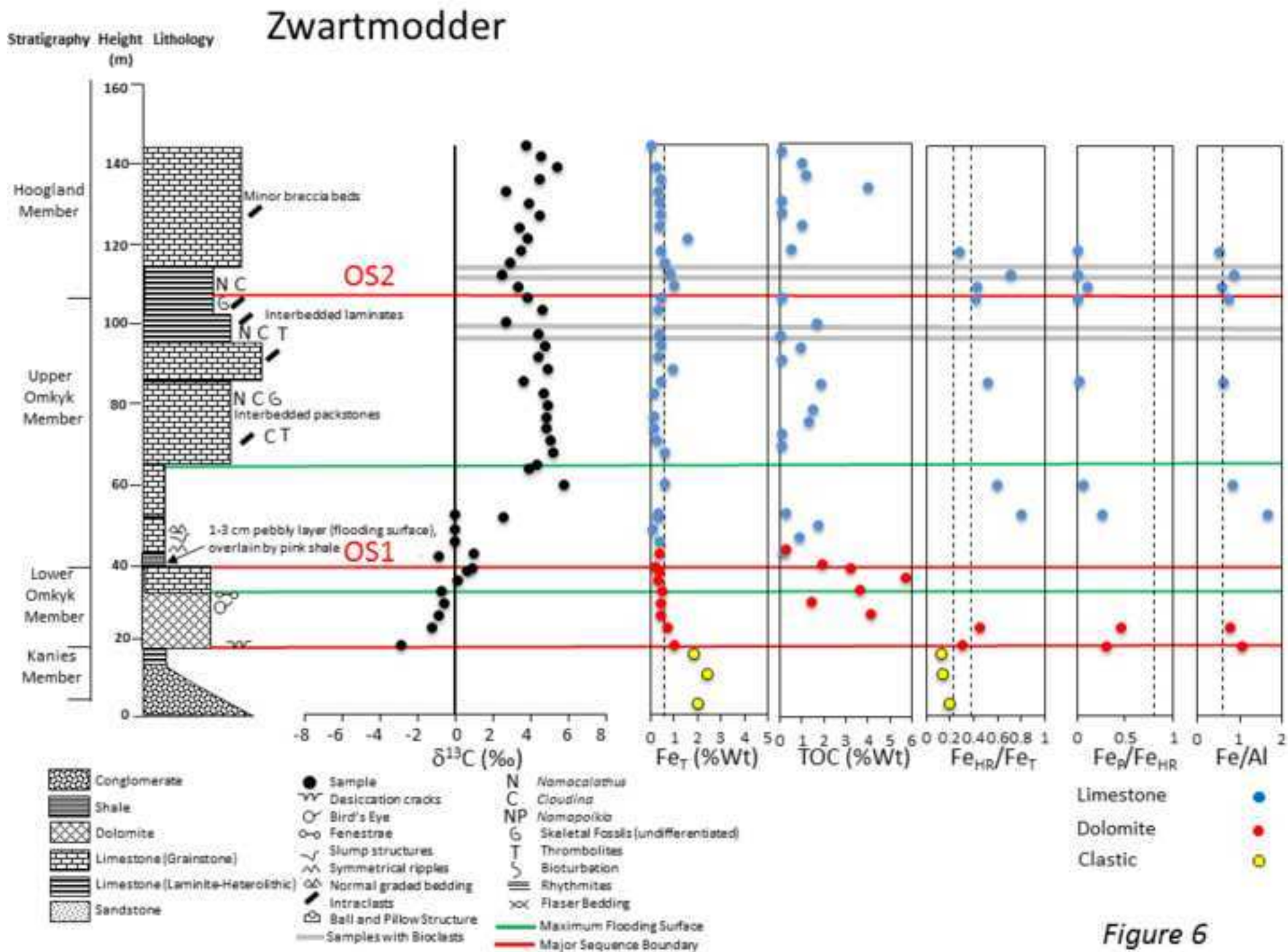


Figure 6

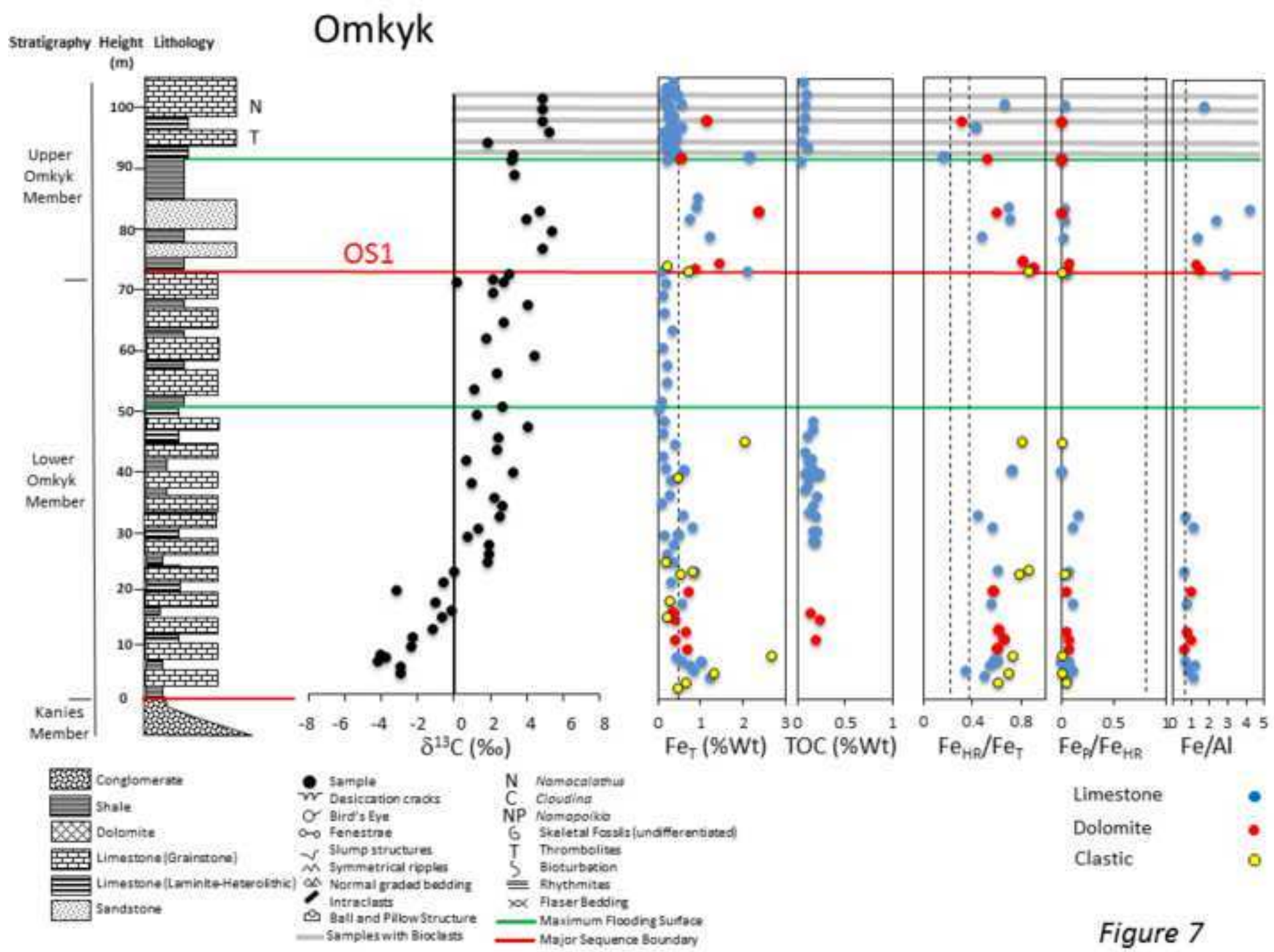


Figure 7

Figure 8

Zebra River

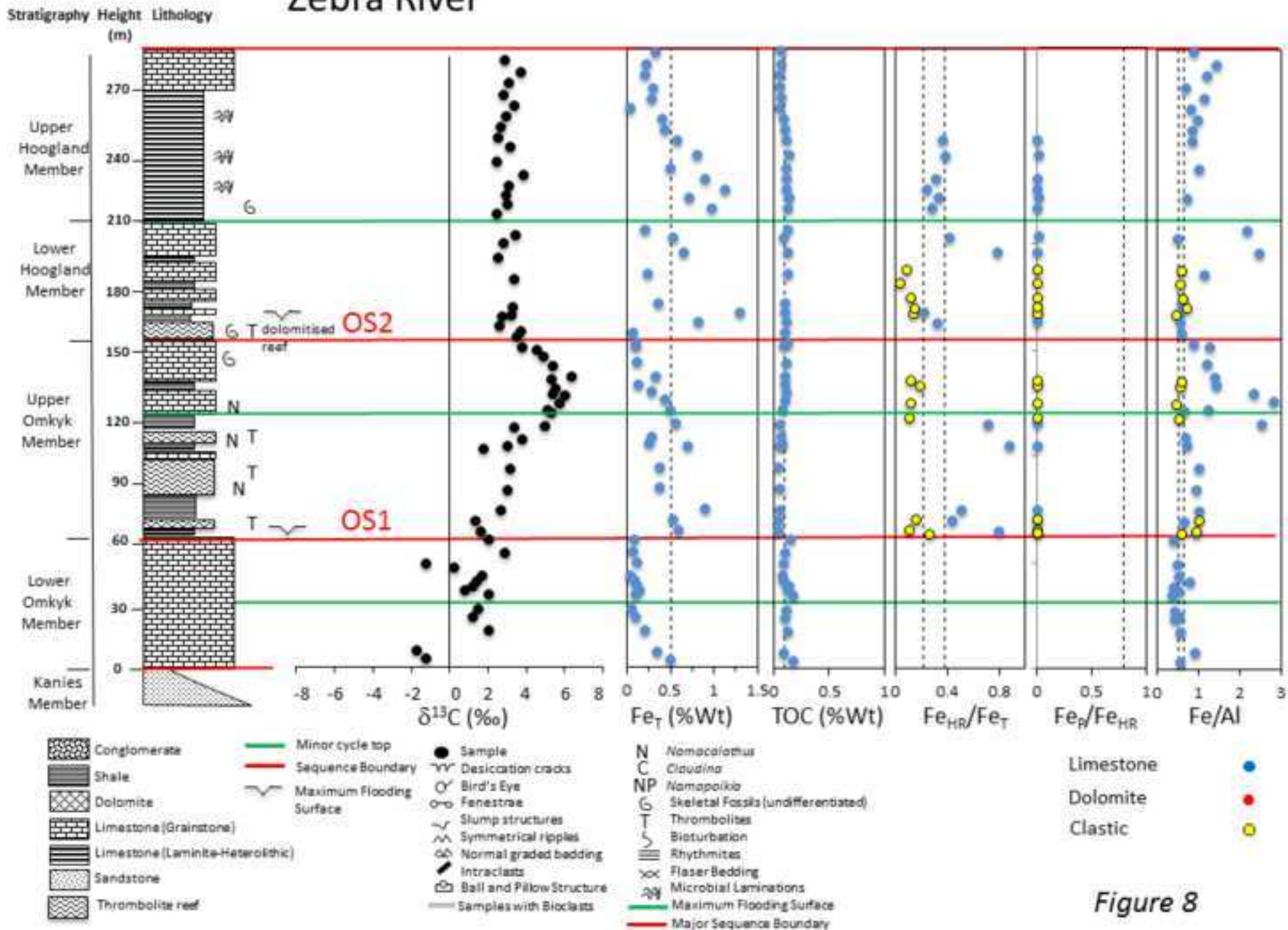


Figure 8

Figure 9

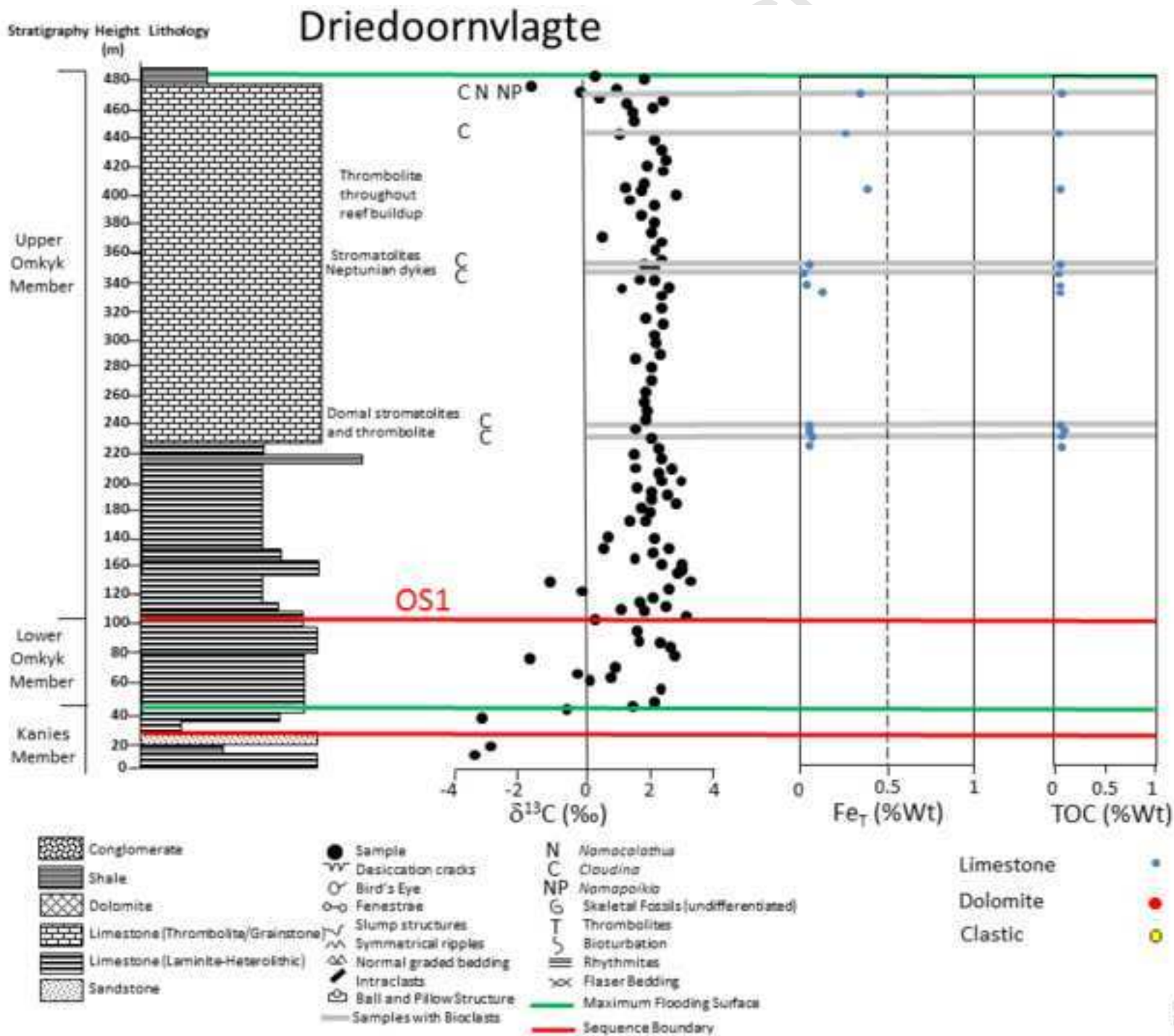


Figure 9

Figure 10

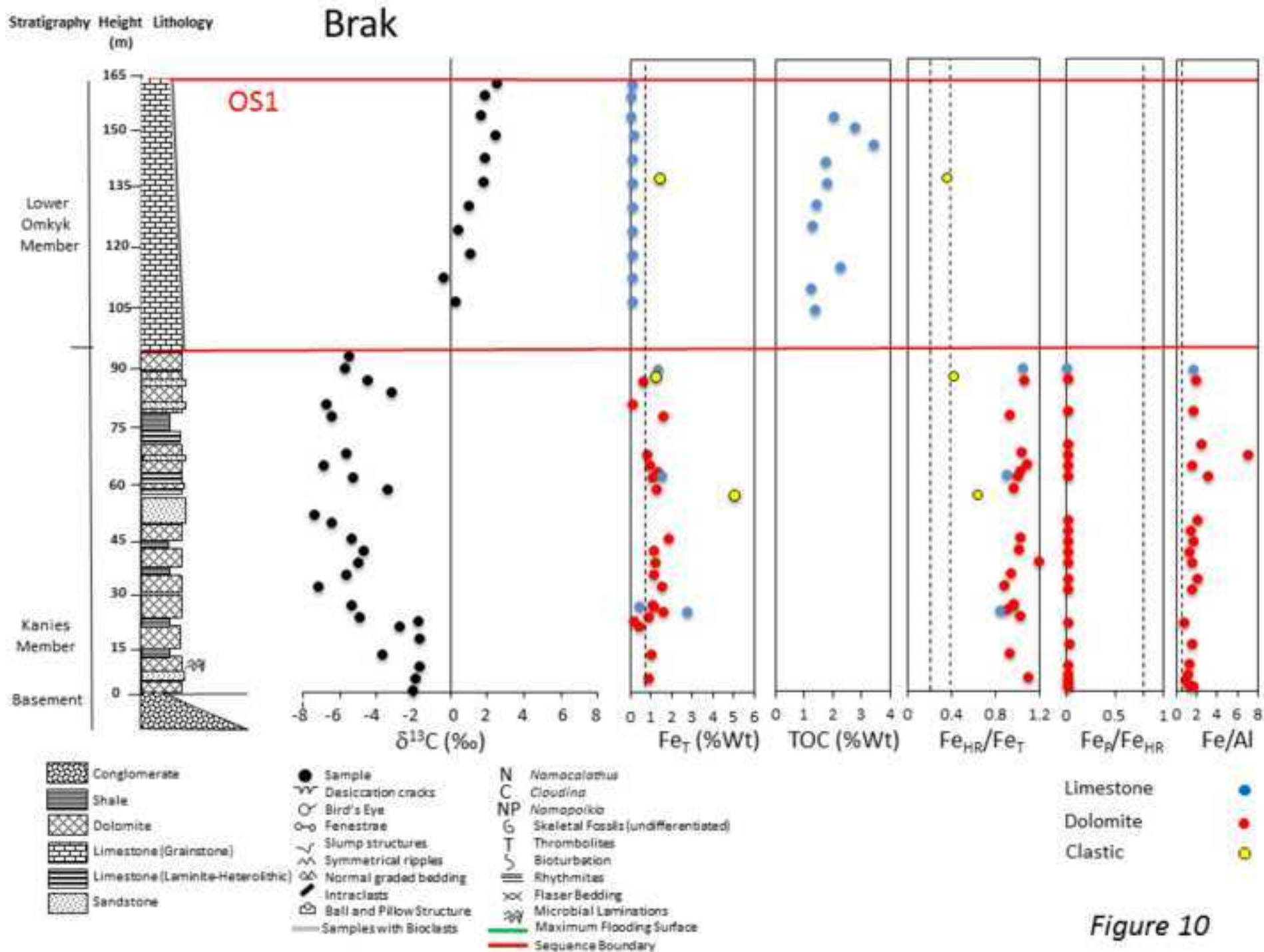


Figure 10

Figure 11

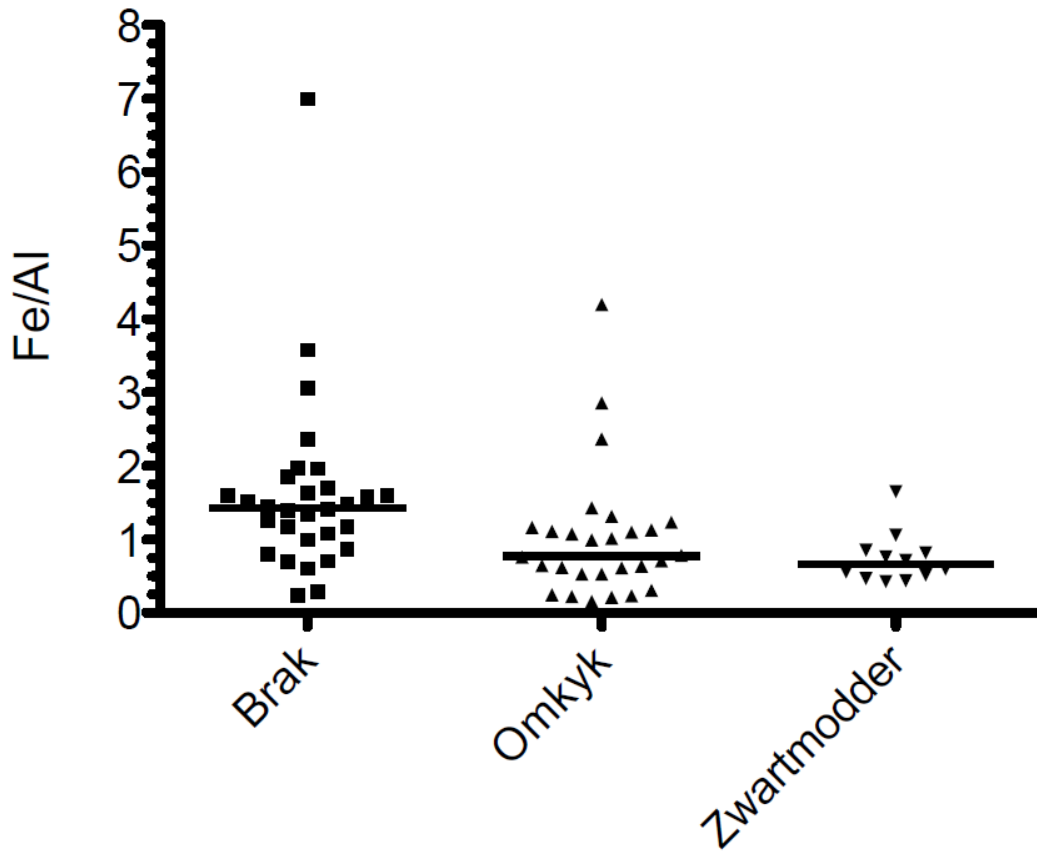


Figure 11

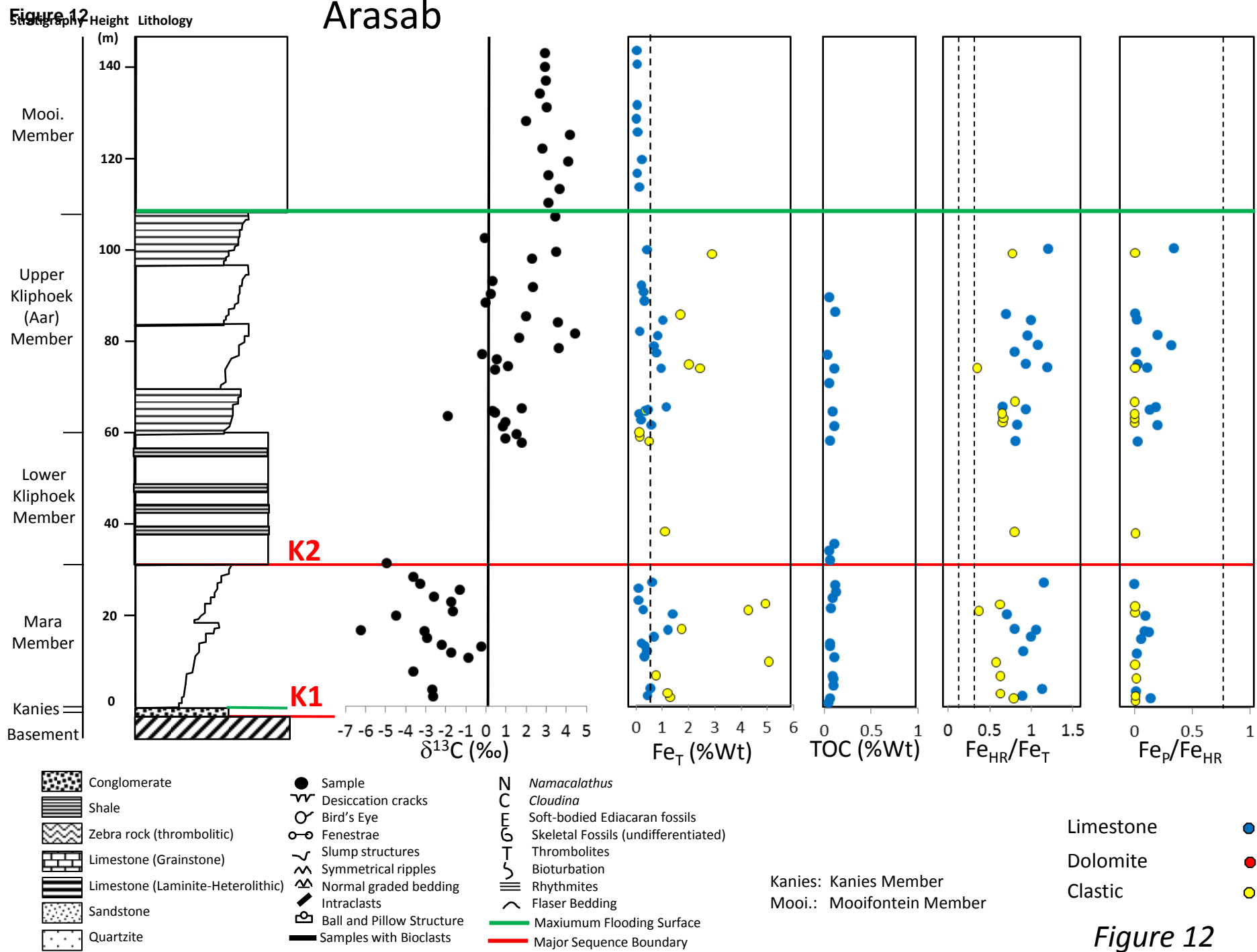
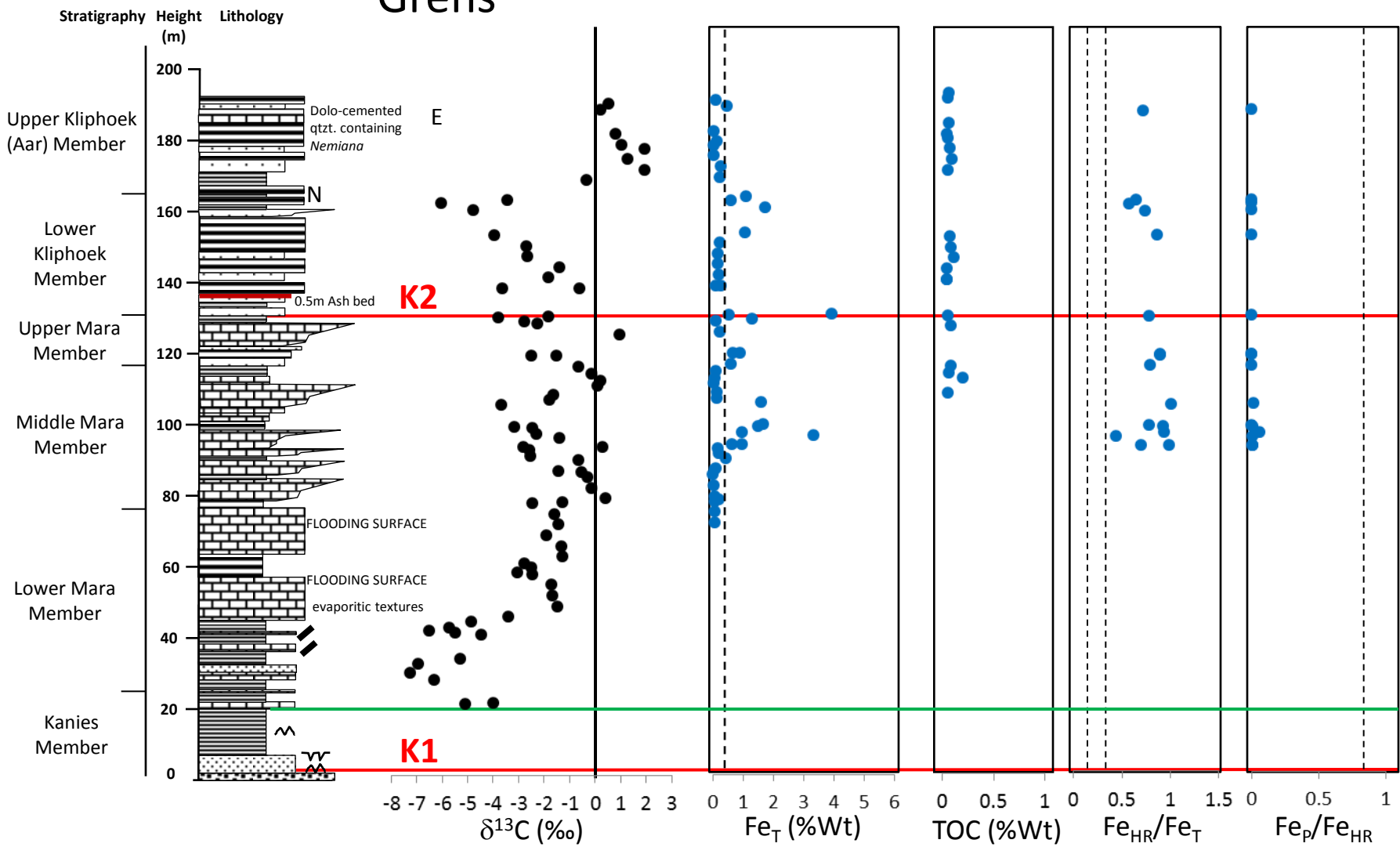


Figure 12

Figure 13

Grens



- Conglomerate
- Shale
- Zebra rock (thrombolitic)
- Limestone (Grainstone)
- Limestone (Laminite-Heterolithic)
- Sandstone
- Quartzite

- Sample
- Desiccation cracks
- Symmetrical ripples
- Intraclasts
- Samples with Bioclasts
- Bioturbation
- Rhythmites
- Flaser Bedding

- N** *Namacalathus*
- C** *Cloudina*
- E** Soft-bodied Ediacaran fossils
- G** Skeletal Fossils (undifferentiated)
- T** Thrombolites

- Maximum Flooding Surface
- Major Sequence Boundary

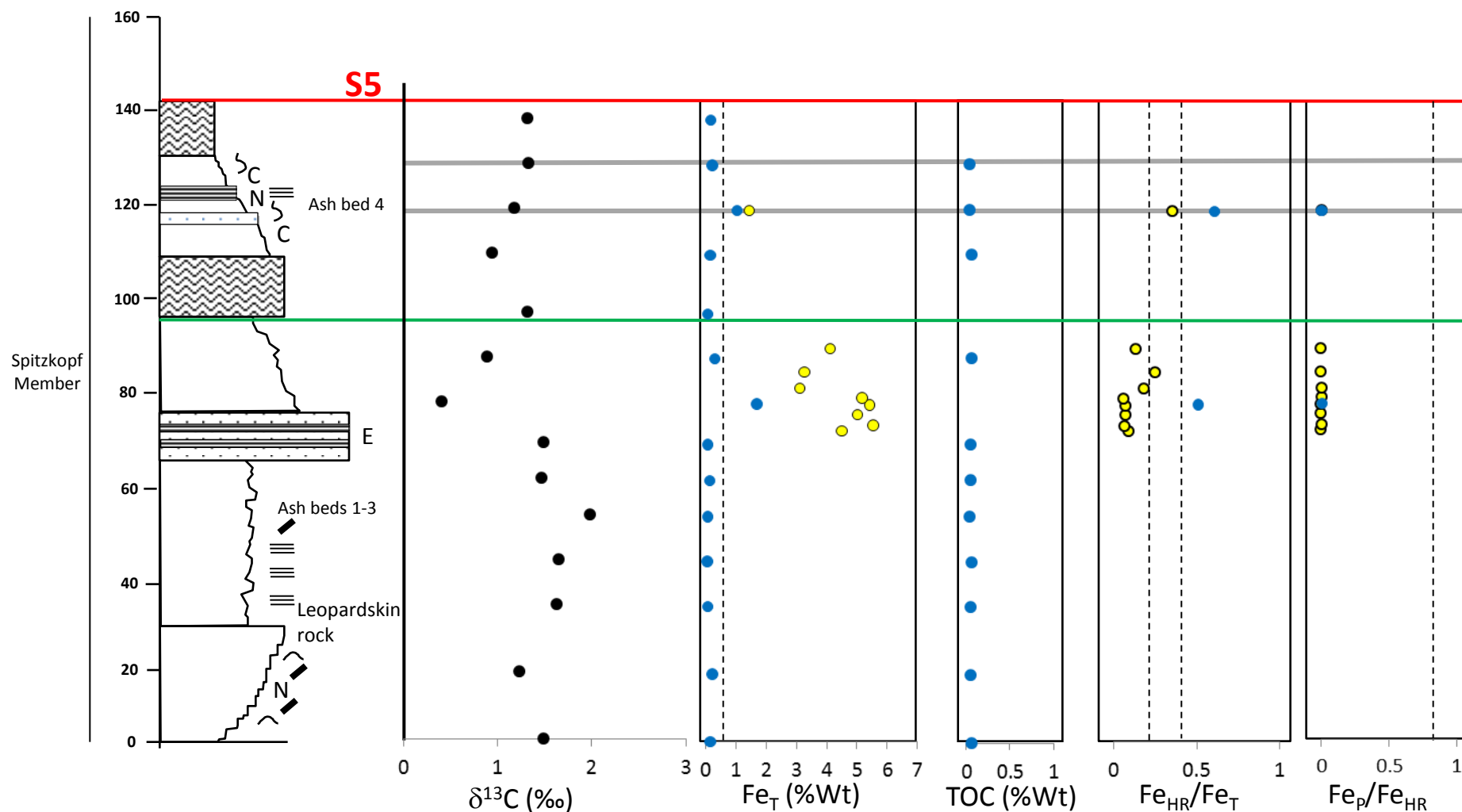
- Limestone
- Dolomite
- Clastic

Figure 13

Figure 14

Swartpunt

Stratigraphy Height (m) Lithology



Spitzkopf Member

- Conglomerate
- Shale
- Zebra rock (thrombolitic)
- Limestone (Grainstone)
- Limestone (Laminite-Heterolithic)
- Sandstone
- Quartzite

- Sample
- Desiccation cracks
- Bird's Eye
- Fenestrae
- Slump structures
- Symmetrical ripples
- Normal graded bedding
- Intraclasts
- Ball and Pillow Structure
- Samples with Bioclasts

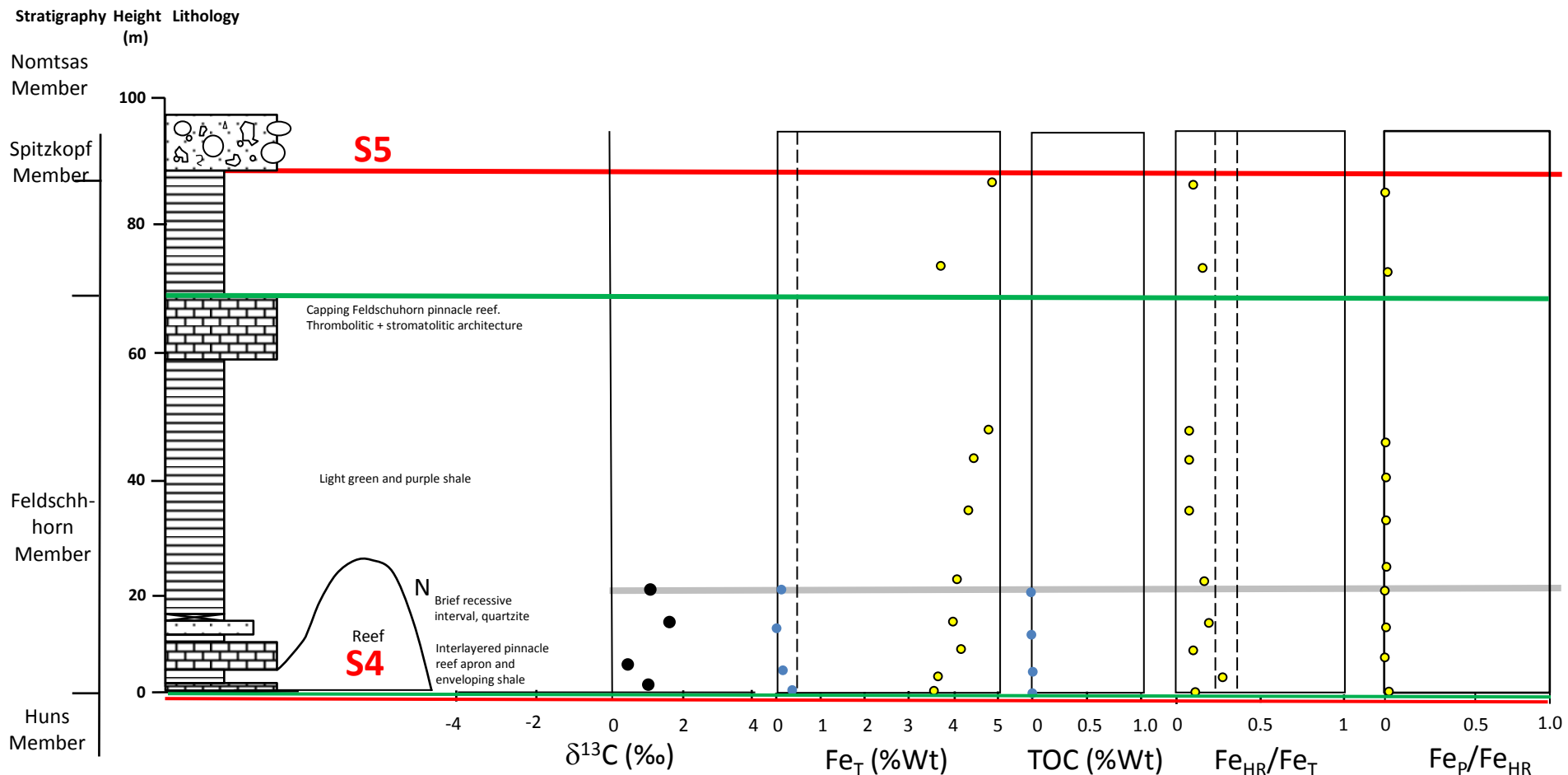
- N** *Namacalathus*
- C** *Cloudina*
- E** Soft-bodied Ediacaran fossils
- G** Skeletal Fossils (undifferentiated)
- T** Thrombolites
- S** Bioturbation
- Rhythmites
- Flaser Bedding
- Minor Maximum Flooding Surface
- Major Sequence Boundary

- Limestone
- Dolomite
- Clastic

Figure 14

Figure 15

Pinnacle Reefs



- | | | | | | |
|-----------------|-----------------------------------|--|---------------------------|-----------|-------------------------------------|
| | Conglomerate | | Sample | N | <i>Namacalathus</i> |
| | Shale | | Desiccation cracks | C | <i>Cloudina</i> |
| | Dolomite | | Bird's Eye | NP | <i>Namapoikia</i> |
| | Limestone (Grainstone) | | Fenestrae | G | Skeletal Fossils (undifferentiated) |
| | Limestone (Laminite-Heterolithic) | | Slump structures | T | Thrombolites |
| | Sandstone | | Symmetrical ripples | S | Bioturbation |
| Minor Cycle Top | | | Normal graded bedding | | Rhythmites |
| | | | Intraclasts | | Flaser Bedding |
| | | | Ball and Pillow Structure | | Maximum Flooding Surface |
| | | | Samples with Bioclasts | | Sequence Boundary |

- | | |
|-----------|--|
| Limestone | |
| Dolomite | |
| Clastic | |

Figure 15

A

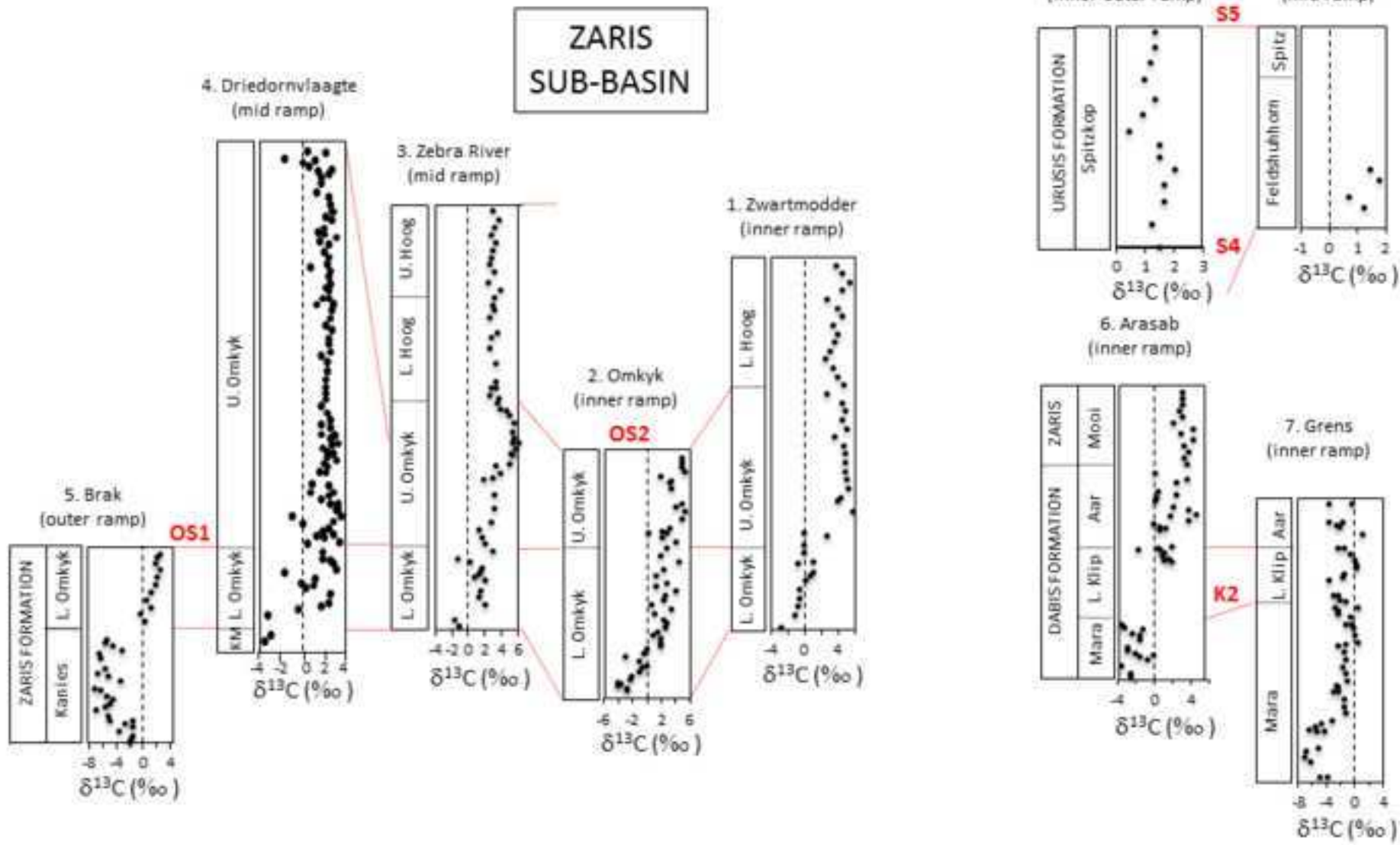


Figure 16A

Figure 16B

B

WITPUTS
SUB-BASIN

ZARIS
SUB-BASIN

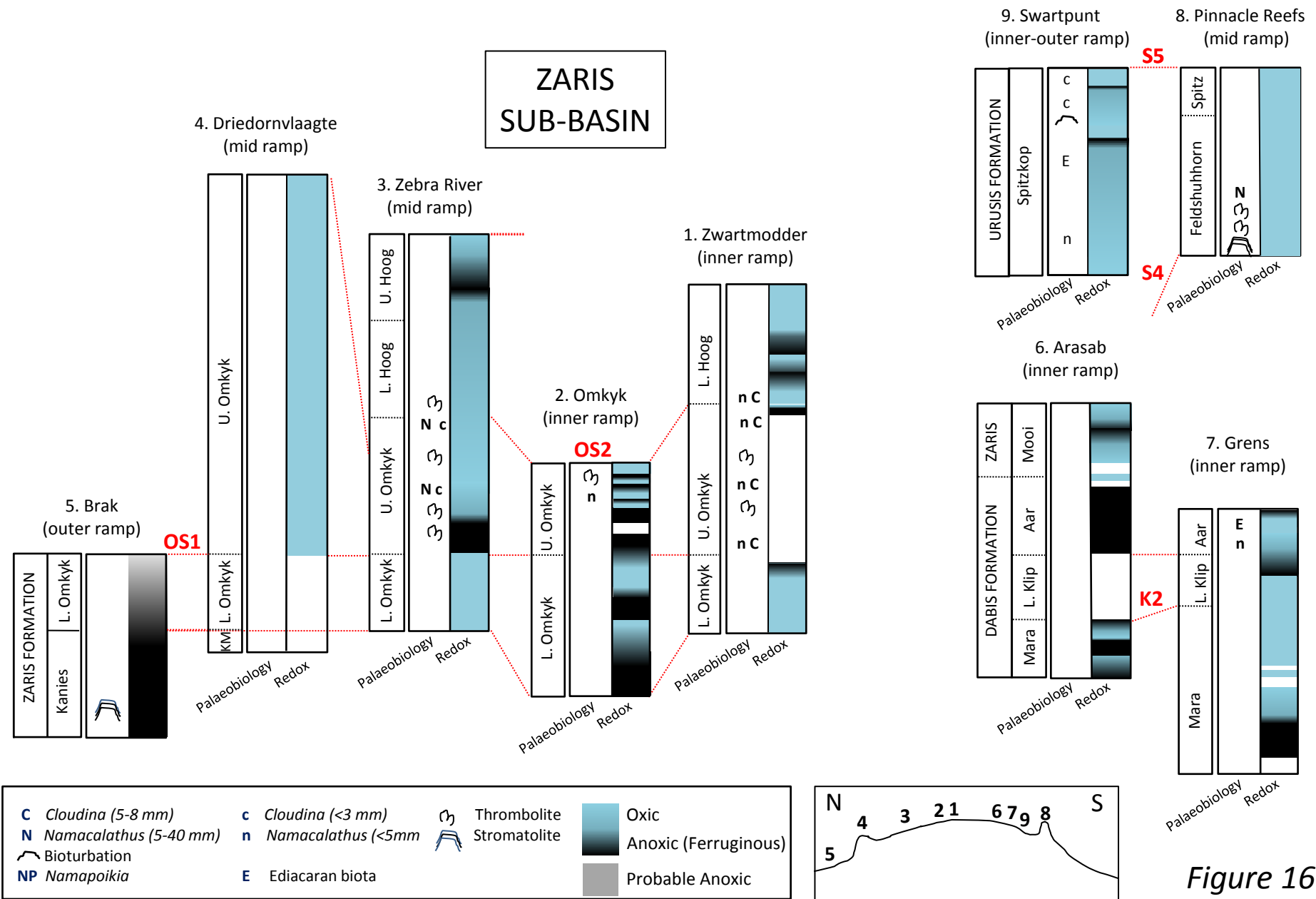


Figure 16B

Figure 17

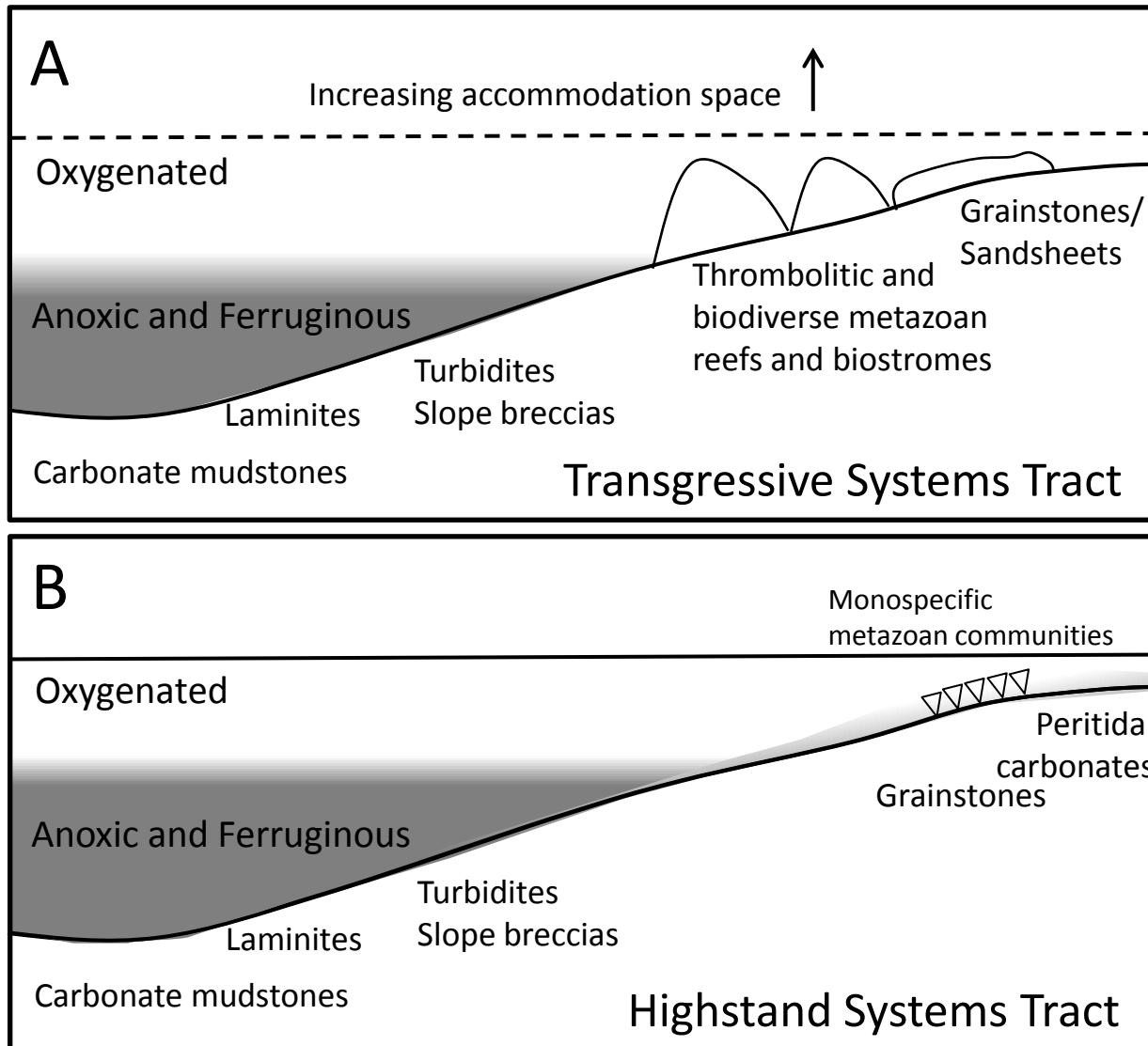
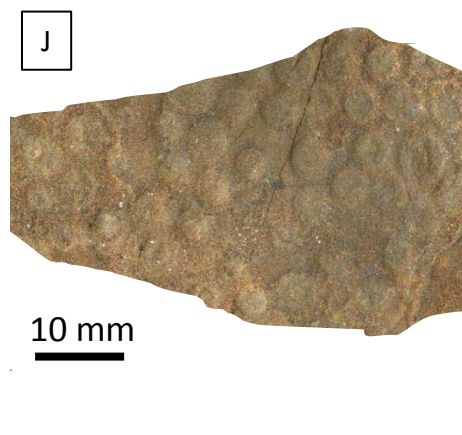
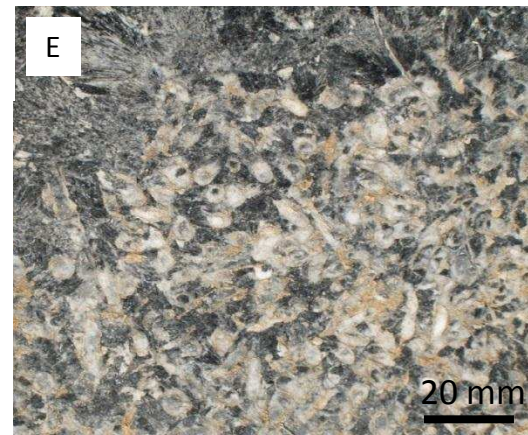
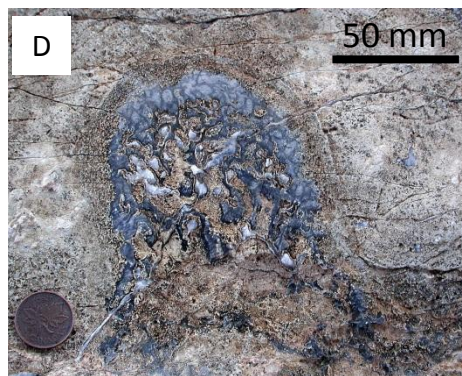
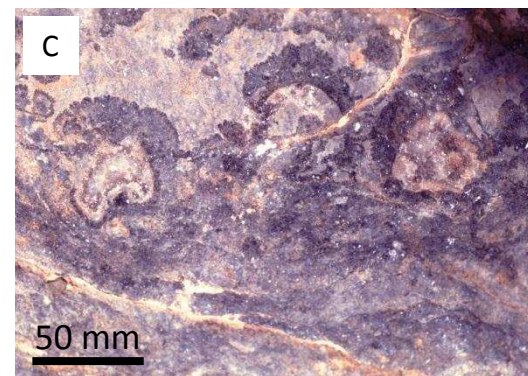
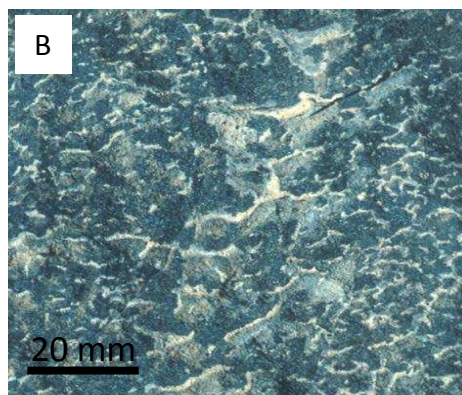


Figure 17

Figure 18 Persistent Oxia



Impersistent Oxia

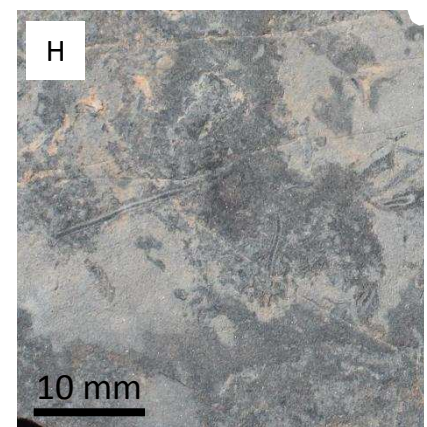
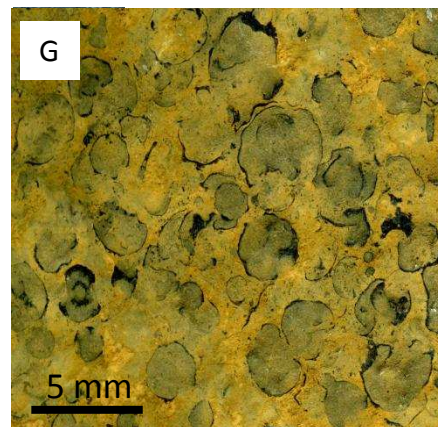
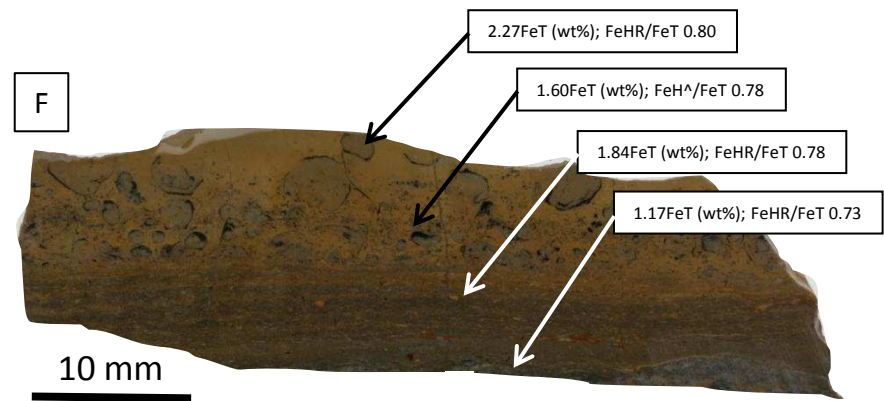


Figure 18